



Budapest University of Technology and Economics
Faculty of Electrical Engineering and Informatics
Department of Automation and Applied Informatics

Study of sensorless PMSM control methods

Scientific Students' Association Report

Author:

Kristóf Oláh

Advisor:

dr. Péter Pál Stumpf

2023

Contents

1	Introduction	1
2	Field-oriented control of Permanent Magnet Synchronous Motors	2
2.1	Coordinate transformations	2
2.2	Permanent Magnet Synchronous Motors	3
2.2.1	Mathematical model of PMSMs	4
2.3	Field-oriented control (FOC)	6
3	A review of sensorless methods	9
3.1	Grouping of sensorless methods	9
3.2	Saliency and Signal Injection based methods (Low-speed and standstill)	10
3.2.1	Signal Injection based methods	10
3.2.1.1	Rotating high frequency injection	11
3.2.1.2	Pulse high frequency injection	13
3.2.2	Methods based on monitoring the locus of the stator space vector current	14
3.2.3	Fundamental PWM excitation (FPE) based methods	14
3.2.3.1	Indirect flux detection by on-line reactance measure- ment (INFORM)	14
3.2.3.2	Zero-sequence current derivatives (ZSCD) measure- ment method	15
3.2.3.3	Zero voltage vector injection (ZVVI) method	16
3.3	Fundamental Excitations based methods (Medium and High-speed) .	16
3.3.1	Nonadaptive methods	17

3.3.1.1	Techniques using the measured DC-Link	17
3.3.1.2	Estimators using monitored stator voltages or currents	17
3.3.1.3	Flux based position estimators	18
3.3.1.4	Position estimators based on back-EMF	18
3.3.2	Adaptive methods	20
3.3.2.1	Estimator based on Model Reference Adaptive System (MRAS)	20
3.3.2.2	Observer-based estimators	21
3.3.2.3	Kalman Filter and Extended Kalman Filter (EKF)	25
3.4	Artificial Intelligence based methods	26
4	A proposed wide-speed-range sensorless control method	28
4.1	Initial position estimation: DC pulse injection	28
4.2	Low-speed control: High frequency alternating signal injection	29
4.3	High-speed control: Luenberger observer	31
4.3.1	State space model of the observer	32
4.3.2	Observer design	35
4.3.3	Discretized Luenberger observer	35
4.3.4	Extraction of rotor speed and position	36
4.4	Combining sensorless control methods	37
5	Simulation of sensorless methods	38
5.1	Overview of the simulation	38
5.1.1	Environment	38
5.1.2	Machine parameters	39
5.1.3	Control loop without estimation	40
5.2	High frequency alternating signal injection	41
5.2.1	Structure of the simulation model	42
5.2.2	Results of the simulation	43
5.3	Luenberger observer	47

5.3.1	Observer design	47
5.3.2	Structure of the simulation model	49
5.3.3	Results of the simulation	49
5.3.3.1	Open-loop operation	50
5.3.3.2	Advanced Luenberger observer	50
5.3.3.3	Simplified Luenberger observer	52
5.3.3.4	Parameter sensitivity tests	53
5.4	Combining the estimators	56
6	Implementation	60
	Bibliography	63

Chapter 1

Introduction

In modern electric drives mostly permanent magnet machines are used. When we control these types of motors, we want to get the most out of them, our goal is the greatest possible torque with the least loss. Field-oriented control (FOC) provides all of this for us, but to implement this control process the position information of the rotor is required. Usually, not only current control, but speed control is also necessary, then the actual angular velocity of the rotor needs to be determined as well. Even though these values can be measured by different sensors, sometimes either the placement of these sensors is difficult or even impossible due to the physical design of the machine, or some companies want to save on the cost of the sensors. In this case position and speed sensorless techniques can be used to determine the necessary information.

This report will present several existing sensorless methods that can be found in the literature and propose a combination of estimators, in order to present a control method that is functioning the entire operational speed range. These estimators will be implemented and tested in MATLAB/Simulink environment.

First, in chapter 2 permanent magnet synchronous machines will be presented including their mathematical model, then the theory of FOC will be shown. In chapter 3 a review will be given of the existing sensorless methods, while in chapter 4 the theory of the chosen estimators will be discussed in detail. After the theoretical part of the sensorless methods are known the simulations will be presented in chapter 5, where both estimators will be investigated individually and then their combination will be shown. Finally, the further work will be discussed briefly in chapter 6.

Chapter 2

Field-oriented control of Permanent Magnet Synchronous Motors

2.1 Coordinate transformations

During the control of PMSMs several coordinate systems need to be used in order to make calculations and the control process easier. These coordinate systems can be transformed into each other, these transformations will be presented in this section.

The abc reference frame describes the 3-phase model of the machine, where the phase vectors are shifted 120 degrees each other. First, by applying the so-called Clarke transform, a two-phase stationary reference frame (SRF), called α - β frame is obtained, where instead of the three, only two phase vectors are used, shifted 90 degrees each other. The Clarke transform (2.1) and its inverse (2.2) are described with the following equations.

$$\begin{bmatrix} i_\alpha \\ i_\beta \end{bmatrix} = T_{Clarke} \begin{bmatrix} i_a \\ i_b \\ i_c \end{bmatrix} = \frac{2}{3} \begin{bmatrix} 1 & -\frac{1}{2} & -\frac{1}{2} \\ 0 & \frac{\sqrt{3}}{2} & -\frac{\sqrt{3}}{2} \end{bmatrix} \begin{bmatrix} i_a \\ i_b \\ i_c \end{bmatrix} \quad (2.1)$$

$$\begin{bmatrix} i_a \\ i_b \\ i_c \end{bmatrix} = T_{Clarke}^{-1} \begin{bmatrix} i_\alpha \\ i_\beta \end{bmatrix} = \frac{2}{3} \begin{bmatrix} 1 & 0 \\ -\frac{1}{2} & \frac{\sqrt{3}}{2} \\ -\frac{1}{2} & -\frac{\sqrt{3}}{2} \end{bmatrix} \begin{bmatrix} i_\alpha \\ i_\beta \end{bmatrix} \quad (2.2)$$

Secondly, if one further transformation, the Park transform is applied on the previous reference frame we get into the d - q rotating reference frame (RRF). It has also

two phase vectors shifted by 90 degrees relative to each other, but rotating with synchronous angular speed. The Park transform (2.3) and its inverse (2.4) are written as

$$\begin{bmatrix} i_d \\ i_q \end{bmatrix} = T_{Park} \begin{bmatrix} i_\alpha \\ i_\beta \end{bmatrix} = \begin{bmatrix} \sin(\theta_e) & -\cos(\theta_e) \\ \cos(\theta_e) & \sin(\theta_e) \end{bmatrix} \begin{bmatrix} i_\alpha \\ i_\beta \end{bmatrix} \quad (2.3)$$

$$\begin{bmatrix} i_\alpha \\ i_\beta \end{bmatrix} = T_{Park}^{-1} \begin{bmatrix} i_d \\ i_q \end{bmatrix} = \frac{2}{3} \begin{bmatrix} \sin(\theta_e) & \cos(\theta_e) \\ -\cos(\theta_e) & \sin(\theta_e) \end{bmatrix} \begin{bmatrix} i_d \\ i_q \end{bmatrix} \quad (2.4)$$

where θ_e is the actual electrical position of the rotor, which can be expressed as $P\Theta_m$, where Θ_m is the mechanical angle of the machine and P is the number of pole pairs. Figure 2.1 illustrates the aforementioned coordinate systems in case of a two-pole machine.

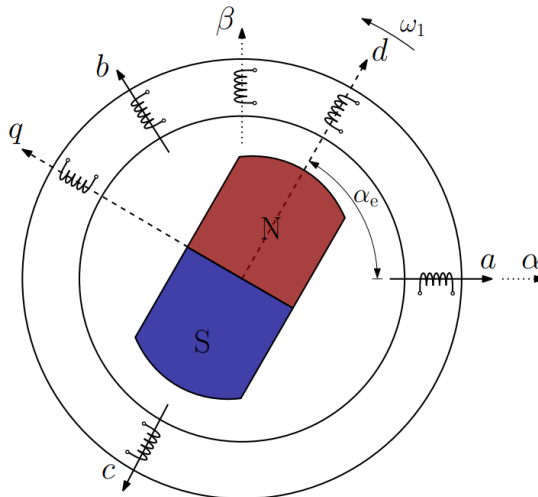


Figure 2.1: Representation of the abc axes, the α - β SRF and the d - q RRF of a two-pole PMSM.

2.2 Permanent Magnet Synchronous Motors

Permanent Magnet Synchronous Motors are machines equipped with permanent magnets in their rotors. PM motors have two types based on the shape of the Back Electro-Motive Force (BEMF) signal. We can talk about BLDCs when the signal is trapezoidal and PMSMs in case of sinusoidal signal shapes. The stator of these electric drives has 3-phase windings, these can be supplied from an inverter.

PMSMs have two common types which are differentiated based on how the permanent magnets are placed on the rotor, this is presented on figure 2.2.

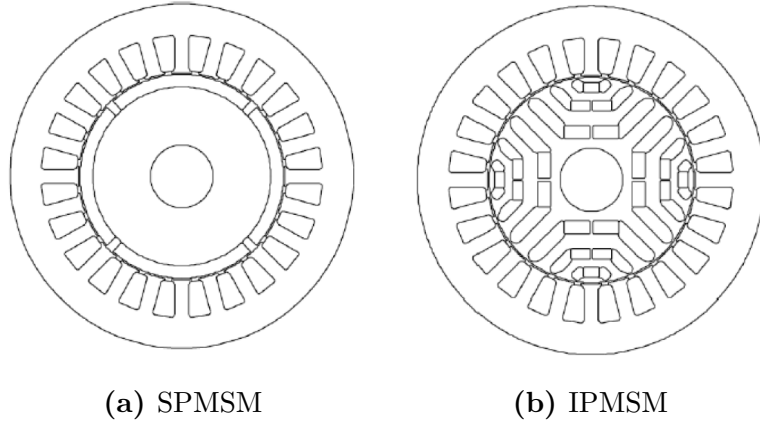


Figure 2.2: Different types of PMSMs based on the positioning of the magnets.

When the magnets are installed on the surface of the rotor we can talk about surface mounted PM motors (SPMSM). This type has an approximately isotropic rotor surface and structural saliency does not really appear in this case. The machine is symmetrical from the inductance point of view, the L_d and L_q inductances are the same.

The other type is the interior PM motors (IPMSMs), where the magnets are installed lowered into the rotor. In this case the machine is highly anisotropic and the effect of saliency is significant. At this type of machine the inductances are highly different, the q -axis inductance is higher than the d -axis one, $L_q > L_d$. The advantage of IPMSM is that the torque of the electric machine can be increased with the reluctance torques, when the rotor is anisotropic. At vehicle drive systems the torque can be increased by even 50% [20].

2.2.1 Mathematical model of PMSMs

The mathematical model of PMSMs can be expressed in all three reference frames. The abc reference frame describes the 3-phase model of the machine, based on [1] the 3-phase voltages of a PMSM machine can be written as

$$\begin{aligned}
 v_a &= R_s i_a + \frac{d}{dt} \psi_a \\
 v_b &= R_s i_b + \frac{d}{dt} \psi_b \\
 v_c &= R_s i_c + \frac{d}{dt} \psi_c
 \end{aligned} \tag{2.5}$$

where v_a, v_b, v_c are the phase voltages, i_a, i_b, i_c are the phase currents, ψ_a, ψ_b, ψ_c are the phase flux linkages and R_s is the stator phase resistance.

When the Clarke transform is applied and the model is transformed into the α - β stationary reference frame, instead of the three, only two phase vectors are used, shifted 90 degrees each other. Writing the 2-phase voltage equations in the α - β SRF [12] gives us the following form

$$\begin{aligned}
v_\alpha &= R_s i_\alpha + \frac{d}{dt} \psi_\alpha \\
v_\beta &= R_s i_\beta + \frac{d}{dt} \psi_\beta \\
\psi_\alpha &= L_s i_\alpha + \psi_M \cos(\theta_e) \\
\psi_\beta &= L_s i_\beta + \psi_M \sin(\theta_e)
\end{aligned} \tag{2.6}$$

where ψ_M is the rotor magnetic flux, L_s is the stator phase inductance and θ_e is the angle of the rotor.

Alternatively the equations in the α - β frame can be expressed using the L_d , L_q inductances and the electrical angular frequency (ω_e). Based on [4, 9] it can be written as

$$\begin{aligned}
v_\alpha &= R_s i_\alpha + \frac{d}{dt} L_\alpha i_\alpha + \frac{d}{dt} L_{\alpha\beta} i_\beta - \omega_e \psi_M \sin(\theta_e) \\
v_\beta &= R_s i_\beta + \frac{d}{dt} L_\beta i_\beta + \frac{d}{dt} L_{\alpha\beta} i_\alpha + \omega_e \psi_M \cos(\theta_e)
\end{aligned} \tag{2.7}$$

where

$$\begin{aligned}
L_0 &= (L_d + L_q)/2, \quad L_1 = (L_d - L_q)/2, \\
L_\alpha &= L_0 + L_1 \cos(2\theta_e), \quad L_\beta = L_0 - L_1 \cos(2\theta_e), \quad L_{\alpha\beta} = L_1 \sin(2\theta_e).
\end{aligned}$$

The equations work both for SPMSMs and IPMSMs, but in case of SPMSMs $L_d = L_q = L_s$ inductance must be used. It results that the L_1 and $L_{\alpha\beta}$ terms will be 0, while $L_\alpha = L_\beta = L_0 = L_s$ can be used as the other terms.

If the Park transform is applied on the previous equations the mathematical model of the motor is obtained in the d - q RRF. Based on [16] the voltages of a PMSM in the d - q rotating reference frame can be described with the following equations

$$\begin{aligned}
v_d &= R_s i_d + \frac{d\psi_d}{dt} - \omega_e \psi_q \\
v_q &= R_s i_q + \frac{d\psi_q}{dt} + \omega_e \psi_d \\
\psi_d &= L_d i_d + \psi_M \\
\psi_q &= L_q i_q
\end{aligned} \tag{2.8}$$

or in matrix form it is given as

$$\begin{bmatrix} v_d \\ v_q \end{bmatrix} = \begin{bmatrix} R_s + \frac{d}{dt}L_d & -\omega_e L_q \\ \omega_e L_q & R_s + \frac{d}{dt}L_q \end{bmatrix} \begin{bmatrix} \dot{i}_d \\ \dot{i}_q \end{bmatrix} + \begin{bmatrix} 0 \\ \omega_e \psi_M \end{bmatrix}. \quad (2.9)$$

The electrical torque can be written as the following

$$T_e = \frac{3}{2}P[\psi_M i_q - (L_q - L_d)i_d i_q]. \quad (2.10)$$

and the electrical angular position of the rotor is related to the angular frequency by

$$\frac{d\theta}{dt} = \omega_e = P\Omega \quad (2.11)$$

where ω_e is the electrical speed, while Ω is the mechanical angular frequency. L_d and L_q are d and q axis inductances and P is the number of pole pairs. At PMSMs most of the natural magnetic flux is on the d axis, hence i_d needs to be set around 0.

In general, PMSMs require constant torque performance at low speed and a constant power at higher speeds. Typically two operating regions can be classified. Below the nominal speed, the machine operates in the so-called constant torque region, while above the base speed in the so-called field weakening or constant power region.

In the constant torque region, the d axis current of SPMSM is controlled to be zero and the q axis current is proportional to the electrical torque. In the case of IPMSM the d and q axis current values are typically obtained by the MTPA (Maximum torque per Ampere) scheme by using the following equations

$$\begin{aligned} i_{d_MTPA} &= -\frac{\psi_M}{4(L_d - L_q)} - \sqrt{\frac{\psi_M^2}{16(L_d - L_q)^2} + \frac{i_{max}^2}{2}} \\ i_{q_MTPA} &= \sqrt{i_{max}^2 - (i_{d_MTPA})^2}. \end{aligned} \quad (2.12)$$

2.3 Field-oriented control (FOC)

Field-oriented control is a variable-frequency drive control method, where transformations are applied on the motor's three-phase AC current values in order to control the electric machine using DC-like values. The method was introduced by Hasse and Blaschke in the late 60s.

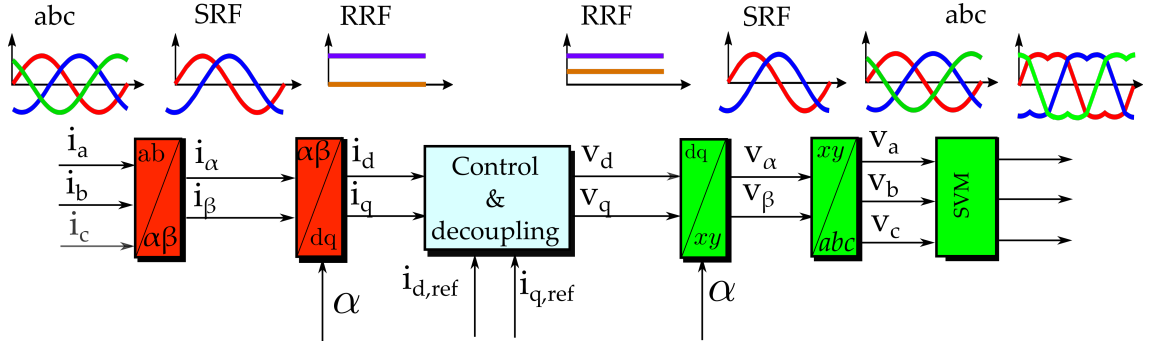


Figure 2.3: Coordinate transformations during an FOC cycle.

In order to make the control easier the 3-phase machine model can be transformed into the 2-phase orthogonal RRF, where the stator currents are DC-like values instead of the fundamental sinusoidal components. This makes a lot easier to implement current controllers for the system as regular PI controllers can be used effectively in case of controlling DC-like values. After the application of the transformations we get two orthogonal components in a rotating frame, which is linked to the rotor of the motor. The direct (d) component corresponds to the flux of the electric drive, meanwhile the quadrature (q) current component stands for the torque. The transformation process and the voltage and current wave forms are presented on figure 2.3.

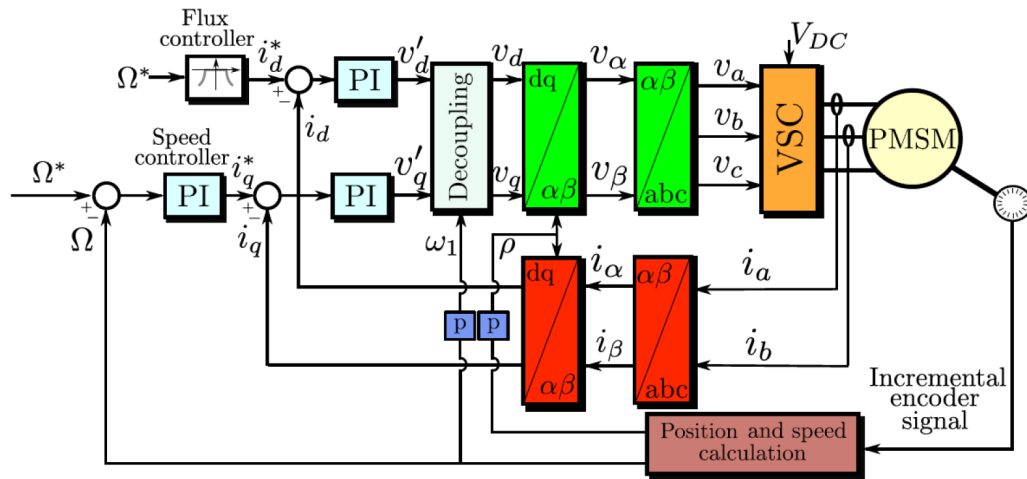


Figure 2.4: A basic example of a FOC machine control.

With FOC we are able to control the i_d and i_q values easily; using e.g., PI controllers, the measured currents can be kept at their reference values. An example of this process is presented on figure 2.4. To validate the values of i_d and i_q and apply our changes to the real machine firstly we need to do the inverse transformations on the controllers' output signals, in order to get back from the d - q RRF to the

abc reference frame. After that, to generate the appropriate output voltages, a Pulse Width Modulated (PWM) Voltage Source Converter (VSC) is used. The switching signals of the converter typically are generated by the Space Vector Modulation (SVM) scheme.

Chapter 3

A review of sensorless methods

Sensorless speed and position estimators for electric machines is a well-studied field. Over the years numerous methods have been shown and examined in detail. As a reason of the variety of these methods this chapter gives a review for the reader to have a broad view before some estimators are discussed in detail. The methods will be presented and grouped based on previous studies.

3.1 Grouping of sensorless methods

In previous literature several different groupings can be found, but the common in most of the articles is that there are three main categories, with various subcategories. The three main categories based on [1, 2, 3, 16, 14]:

1. Saliency and Signal Injection
2. Fundamental Excitations
 - (a) Nonadaptive Methods
 - (b) Adaptive Methods
3. Artificial Intelligence

The main categories can be called differently such as Saliency-based and Model-based in [25], but the basis of the grouping is the same as in the aforementioned list, that first group of methods work at low-speed while the second group at medium and high-speed range. Figure 3.1 summarize the methods that will be presented later in this chapter.

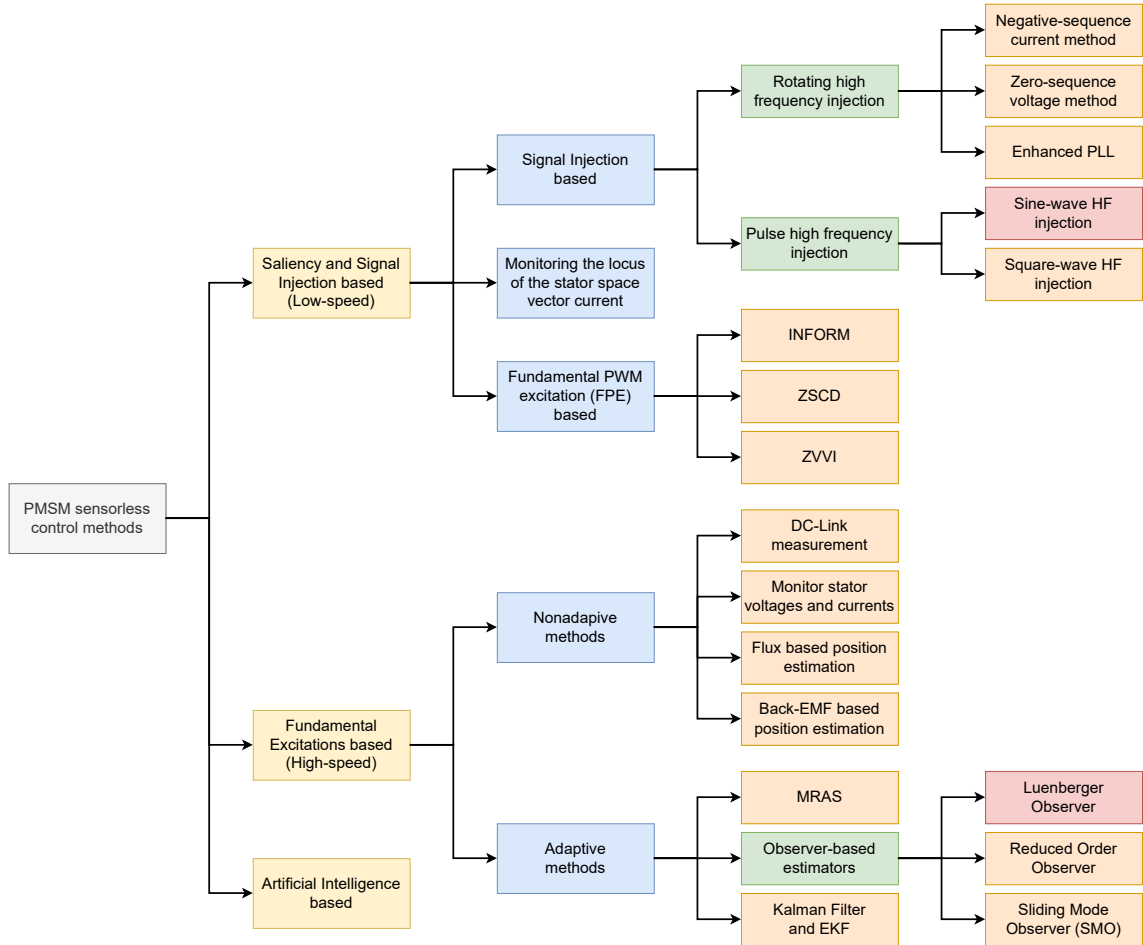


Figure 3.1: Grouping of sensorless methods. The later implemented methods are marked red.

3.2 Saliency and Signal Injection based methods (Low-speed and standstill)

At medium and high-speed ranges Model-Based methods can be implemented using the electromotive force (EMF) or flux associated with the fundamental excitation, but at lower speeds these estimators are not able to operate as a reason of low signal-to-noise-ratio caused by modeling uncertainty, nonlinearities, etc. [25] Zero to low speed range is where Saliency-Based methods can be used, such as signal injection, inductance variation-based methods and others.

3.2.1 Signal Injection based methods

Signal injection based methods widely used at low-speed sensorless control. An additional high frequency signal can be injected into the motor in order to determine the position of the rotor by measuring and processing the change of the injected

signal. Based on [25] the high frequency model of PMSMs in the d - q and in the α - β frame can be described as

$$\begin{bmatrix} v_{d_h} \\ v_{q_h} \end{bmatrix} = \begin{bmatrix} L_d & 0 \\ 0 & L_q \end{bmatrix} \frac{d}{dt} \begin{bmatrix} i_{d_h} \\ i_{q_h} \end{bmatrix} \quad (3.1)$$

$$\begin{bmatrix} v_{\alpha_h} \\ v_{\beta_h} \end{bmatrix} = \begin{bmatrix} L_0 + L_1 \cos(2\theta_e) & L_1 \sin(2\theta_e) \\ L_1 \sin(2\theta_e) & L_0 - L_1 \cos(2\theta_e) \end{bmatrix} \frac{d}{dt} \begin{bmatrix} i_{\alpha_h} \\ i_{\beta_h} \end{bmatrix} \quad (3.2)$$

where θ_e is the rotor position, L_d and L_q are the d and q -axis inductances and $L_0 = (L_d + L_q)/2$ and $L_1 = (L_d - L_q)/2$. Letter h notes the high frequency components. Injection methods can be grouped based on which axis the additional signal is injected into.

3.2.1.1 Rotating high frequency injection

When a rotating high frequency space vector is injected into the α - β frame we can talk about rotating signal injection. The additional signal can be written as eq. 3.3, where V_{rot_h} is the amplitude of the injected component.

$$v_{inj} = \begin{bmatrix} v_{\alpha_h} \\ v_{\beta_h} \end{bmatrix} = V_{rot_h} \begin{bmatrix} \cos(\omega_h t) \\ \sin(\omega_h t) \end{bmatrix} \quad (3.3)$$

The angular frequency of the injected signal (ω_h) is set around one tenth of the PWM switching frequency to ensure that the shape of the injected sinusoidal signal remains recognizable. To process the signal and extract the estimated rotor position two typical methods are used, the negative-sequence current method and zero-sequence voltage method.

Negative-sequence current method

If eq. 3.3 and eq. 3.2 are substituted from each other the response of the currents can be written as

$$\begin{bmatrix} i_{\alpha_h} \\ i_{\beta_h} \end{bmatrix} = \begin{bmatrix} I_{s_p} \sin(\omega_h t) + I_{s_n} \sin(-\omega_h t + 2\theta_e) \\ -I_{s_p} \cos(\omega_h t) - I_{s_n} \cos(-\omega_h t + 2\theta_e) \end{bmatrix} \quad (3.4)$$

where p and n denotes the positive and negative term of the high frequency response currents. By filtering out the high frequency components in the α - β stationary frame using a HPF and transforming the results into the d - q rotating frame, the expression

of the currents is the following

$$\begin{bmatrix} i_{d^h} \\ i_{q^h} \end{bmatrix} = \begin{bmatrix} I_{s_p} \sin(2\omega_h t) + I_{s_n} \sin(2\theta_e) \\ -I_{s_p} \cos(2\omega_h t) - I_{s_n} \cos(2\theta_e) \end{bmatrix} \quad (3.5)$$

where d^h and q^h notes the high frequency rotating frame. After applying a LPF the estimated rotor position can be written as

$$\theta_e = \frac{1}{2} \arctan \left[-\frac{LPF(I_{d^h})}{LPF(I_{q^h})} \right]. \quad (3.6)$$

Zero-sequence voltage method

The rotor position can also be extracted from the zero-sequence carrier voltage. Based on [25] it can be written as

$$V_{RN} \approx \frac{L_{DC} L_2 V_{rot_h}}{2L_{DC}^2 - \frac{1}{2}L_2^2} \cos(\omega_h t + 2\theta_e) \quad (3.7)$$

where L_{DC} and L_2 are amplitudes of DC and second harmonics of phase self-inductances. From this the function of rotor position can be extracted via the following signal processing, from which the estimated rotor position can be calculated by the arctan of the results.

$$\begin{bmatrix} V_{RN_α} \\ V_{RN_β} \end{bmatrix} = LPF \left(V_{RN} \begin{bmatrix} 2\cos(\omega_h t) \\ 2\sin(\omega_h t) \end{bmatrix} \right) = \frac{L_{DC} L_2 V_{rot_h}}{2L_{DC}^2 - \frac{1}{2}L_2^2} \begin{bmatrix} \cos(2\theta_e) \\ \sin(2\theta_e) \end{bmatrix} \quad (3.8)$$

The drawback of this method is that a balanced resistor network and the access to the the neutral point of the machine are needed to measure the zero-sequence voltage.

Enhanced PLL approach

In [17] a novel enhanced PLL (ePLL) approach is introduced for the signal processing. In the aforementioned conventional methods the use of LPFs causes time delay in the system and compromise the system dynamic and control performance. The newly proposed demodulation process for position estimation can be done without the use of LPFs. Compared to other existing methods the ePLL shows great performance in the experimental results.

3.2.1.2 Pulse high frequency injection

The difference compared to the rotating injection is the frame in which the HF signal is injected into. At pulsating signal injection the additional signal is injected into the d - q rotating frame instead of the α - β axes. In this category the most common methods are the sine-wave HF injection and the square-wave HF injection.

Sine-wave high frequency injection

In this method a high frequency sinusoidal wave is injected either into the d or the q -axis or even into both of them. The injected signal can be extracted from the q -axis current feedback branch in the FOC loop and the rotor position can be estimated after a filtering and processing sequence. The method will be presented in depth in chapter 4, hence I will not go into detail here.

Square-wave high frequency injection

The basic idea of the square-wave injection is really similar to the sine-wave method, but the injected signal has a square shape instead of the sinusoidal one. The advantage of this solution is that the frequency of the injected signal can be higher than in the aforementioned signal injection techniques. The injection can be implemented during the current sampling by updating the PWM twice in a switching period, which results that the acoustic noise of the HF signal can be eliminated virtually.

The response of the currents can be obtained as the following in the d - q reference frame [25]

$$\begin{bmatrix} \dot{i}_{\hat{d}_h} \\ \dot{i}_{\hat{q}_h} \end{bmatrix} = \frac{\int i_{inj} dt}{L_d L_q} \begin{bmatrix} L_0 - L_1 \cos(2\Delta\theta_e) \\ -L_1 \sin(2\Delta\theta_e) \end{bmatrix}. \quad (3.9)$$

It can be seen that the response is an alternating triangular signal in the q -axis current, because the integral of the injected square wave's one period (a positive and a negative constant value following each other) is an increasing and decreasing ramp. From eq. 3.9 the position information can be extracted several ways. Either a PI regulator can be used to force the q -axis HF current response to zero, or the equation can be transformed to the α - β stationary frame where the response currents can be demodulated through a LPF [25].

3.2.2 Methods based on monitoring the locus of the stator space vector current

By applying this estimation method the position of the rotor can be obtained at standstill in case of IPMSM ($L_d < L_q$) machines. In steady state the locus of the space vector of the stator currents in the α - β frame becomes an ellipse. By definition, the d -axis of the rotor points to the north pole of the rotor magnet. If the magnetic saturation is neglected, the equation of the ellipse can be written as

$$Ai_\alpha^2 + 2Hi_\alpha i_\beta + Bi_\beta^2 + 1 = 0. \quad (3.10)$$

From this, the angle of the major axis of the ellipse is the following

$$\theta = \frac{1}{2} \tan^{-1} \left(\frac{2H}{A - B} \right). \quad (3.11)$$

If the stator currents are monitored the A , B and H parameters of the ellipse can be determined and the position of the rotor is $\hat{\theta} = \theta + \gamma_u$, where γ_u is displacement angle caused by the armature impedance [3, 13].

3.2.3 Fundamental PWM excitation (FPE) based methods

The high frequency signal injection techniques are a robust and effective way to estimate the rotor position, but complicated signal processing and filtering needed in order to get an accurate position information. The aim of FPE-based estimators is to simplify the implementation of sensorless control. In this section three common FPE-based methods will be presented.

3.2.3.1 Indirect flux detection by on-line reactance measurement (INFORM)

The first presented method is the INFORM which is the simplest one. The basis of this method is the inductance variation, it uses that the change of magnetic conductivities in d and q -axis depends on the rotor position. If voltage state space phasors are applied in all motor phase directions the current response can be measured and from that the rotor position can be extracted [3]. Test vectors can be injected during the null part of each PWM cycle while another equal vector is injected oppositely to compensate the voltage distortion caused by the last vector. To guarantee the effectiveness of the method three cycles are needed with one measurement each cycle [25].

Based on [25] when the injected voltage signals are

$$v_{\alpha\beta k}^s = V_h e^{jk\frac{2}{3}\pi} \quad (3.12)$$

the current responses can be written as

$$\frac{d}{dt} i_{\alpha\beta k}^s = \frac{1}{L_0 - L_1} \left[L_0 - L_1 e^{j2(\theta_e - jk\frac{2}{3}\pi)} \right] V_h e^{jk\frac{2}{3}\pi} \quad (3.13)$$

where $k = 0, 1, 2$ corresponds to phase a , b and c respectively. Combining these responses from the three cycles an equation for the position can be written as the following.

$$\sum \left(\frac{d}{dt} i_{\alpha\beta k}^s e^{jk\frac{2}{3}\pi} \right) = -\frac{3L_1}{L_0^2 - L_1^2} V_h e^{j2\theta_e} \quad (3.14)$$

Besides the basic usage of INFORM further additions can be done to improve the effectiveness of the method. For example in [8] the INFORM was modified in order to lower current ripples, decrease the switching loss and improve the dynamics. In [18] a modified version of INFORM was introduced that used DC-link measurements only. In this case the voltage space phasors for INFORM-position estimation are applied directly by the inverter by interrupting the PWM-pattern for a specific period of time.

3.2.3.2 Zero-sequence current derivatives (ZSCD) measurement method

In the ZSCD method the voltage test vectors are the six nonzero switching states of the voltage source inverter. The injection is done only for a short time between the normal FOC PWM waveform, the vectors are applied in pairs with the same amplitude and to the opposite direction. The current responses contain the zero sequence components and a Rogowski coil can be used to measure its derivatives. The position information can be calculated as

$$\theta_e = \frac{1}{n} \arctan \left(\frac{P_\beta}{P_\alpha} \right) \quad (3.15)$$

where P is the position scalar and n is the number of saliency cycles per revolution [25].

The advantage of the method is its high performance, but on the other side the drawback is that extra hardware is needed. To excite the zero sequence component

the neutral point of the machine must be accessible which is not achievable in some industrial applications.

3.2.3.3 Zero voltage vector injection (ZVVI) method

The method combines the derivation calculations of current and zero voltage vector injection, which means that between the normal FOC PWM periods additional zero voltage vectors are inserted. This increases the current fluctuation compared to the regular PWM switching sequence but reduces the acoustic noise caused by the injection technique. Based on [25] the rotor position information can be extracted from the voltage equations of the motor during the zero switching period.

$$\left(\frac{di_\alpha}{dt} + \frac{R}{L_q}i_\alpha\right) \sin\theta_e - \left(\frac{di_\beta}{dt} + \frac{R}{L_q}i_\beta\right) \cos\theta_e = \frac{\psi_f}{L_q} \frac{d\theta_e}{dt} \quad (3.16)$$

From the equation it can be seen that the position of the rotor can be extracted by measuring the currents and the current differentials in the α - β stationary frame. The advantage of the the method is that no additional acoustic noise is generated as no additional signal is injected into the system, furthermore the method is not sensitive to parameters' variation.

3.3 Fundamental Excitations based methods (Medium and High-speed)

The aforementioned estimation techniques show great performance at standstill or low speeds, but they have several drawbacks at higher speed ranges. As the speed increases the losses caused by the signal injection become significant, torque ripples and acoustic noise also apply as unwanted side effects.

Hence over a certain speed fundamental excitation or alternatively called model based methods can be used. Mostly the common thing in these estimators is that they can be separated to two parts. The first part is an EMF or flux estimator which output is forwarded to the second part, the speed/position observer. This section presents the estimator techniques in two main groups, firstly the nonadaptive methods will be shown, followed by the adaptive ones.

3.3.1 Nonadaptive methods

Nonadaptive methods use directly the measured currents and voltages and the equations of the PMSM machine. The advantage of these methods is the easy computation and fast response, the calculations cause almost no delay. In order to get the position and speed precisely high accurate motor parameters are required.

3.3.1.1 Techniques using the measured DC-Link

An easy and low-cost way to get feedback from the system is measuring the DC-link current. In [6] two energy optimizing techniques are presented via measuring only the DC-link current of the machine and applying a V/f control. The first one is the minimum input power method, which minimizes the average DC-link current at a fixed voltage. The second one is the power factor method, which is based on the shape of the DC-link current. The shape of the current depends on the phase shift between the stator current and the stator voltage. In this case the optimum is when the current and the voltage are in the same phase.

The main problem of the aforementioned methods is that the control is not robust, easily becomes unstable, hence these estimators can be used only in low dynamic applications.

3.3.1.2 Estimators using monitored stator voltages or currents

If stator voltages or currents are monitored, the position and speed can be expressed from the equations of the PMSM. If the inverse Park and Clarke transforms are applied on the d - q frame equations, we get the following term for the rotor position [1, 16].

$$\theta_e = \arctan \left(\frac{v_b - v_c - R_s(i_b - i_c) - L_d \frac{d}{dt}(i_b - i_c) - \sqrt{3}\omega_e(L_q - L_d)i_a}{\sqrt{3}(v_a - R_s i_a - L_d \frac{d}{dt}i_a) + \omega_e(L_q - L_d)(i_b - i_c)} \right) \quad (3.17)$$

The speed can be calculated as

$$\omega_e = \frac{\sqrt{\left(v_a R_s \frac{d}{dt}i_a\right)^2 + \frac{1}{3} \left[v_b - v_c - R_s(i_b - i_c) - L_d \frac{d}{dt}(i_b - i_c)\right]^2}}{\psi_M}. \quad (3.18)$$

To obtain the initial position of the rotor at $t = 0$, $\omega_e = 0$ needs to be substituted in eq. 3.17.

Although this calculation results quick dynamic response, the method is not robust and very sensitive to measurement noise and inaccurate motor parameters.

3.3.1.3 Flux based position estimators

The biggest advantage of flux based estimator methods is that the line voltages can be used for the estimation process [1]. The phase-voltage equation of the stator can be written as

$$v_s = R_s i_s + \frac{d}{dt} \psi_s \quad (3.19)$$

where v_s is the input voltage, i_s is the current, R_s is the resistance and ψ_s is the flux linkage of the stator [1]. If the previous equation is written on ψ_s we get the following term

$$\psi_s = \int e_s = \int (v_s - R_s i_s) dt + \psi_{s0} \quad (3.20)$$

where e is the BEMF and ψ_{s0} is the initial position for the stator flux. If eq. 3.20 is transformed to other reference frames, the position of the rotor can be determined several ways. In the α - β frame θ_e can be obtained as

$$\theta_e = \arctan \left(\frac{\psi_\alpha - L i_\alpha}{\psi_\beta - L i_\beta} \right) \quad (3.21)$$

where L is the winding inductance [29]. In the d - q rotating frame getting the position is even easier, it can be calculated as

$$\theta_e = \arctan \left(\frac{\psi_d}{\psi_q} \right). \quad (3.22)$$

The problem with the simple flux estimation is the use of the pure integrator that produces cumulative error. Noise also causes problems when this method is implemented, hence the use of adaptive methods is preferred in practice.

3.3.1.4 Position estimators based on back-EMF

Based on [14] several different back-EMF methods can be found in the literature, eg. back-EMF zero-crossing detection (only for BLDCs), back-EMF integration, extended EMF (EEMF) or the third harmonic method. The common in all is that they use the back electromotive force related to the rotational speed of the motor.

In [11] a method is shown where a maximum current decaying interval (MCDI) test cycle is added to the control algorithm. This way the back EMF can be measured in the d - q frame, and from the measured values the rotor angle can be calculated as

$$\theta_e = \arctan\left(\frac{-E_d}{E_q}\right). \quad (3.23)$$

A method is proposed in [7] which determines the back-EMF without voltage probes. Instead of measuring the actual voltages, the reference voltages can be used for determining the BEMF. To get the rotor position the back-EMF was used in the α - β reference frame, while other arguments were in the d - q frame.

$$\theta_e = \arctan\left(\frac{e_\beta}{e_\alpha}\right) - \arctan\left(\frac{\psi_M}{L_q i_q}\right) \quad (3.24)$$

As the back-EMF is a subject to the reference voltages in the α - β frame, the relationship between the actual voltages and the reference ones can be expressed and from that an expression to θ_e can be written as

$$\theta_e = \arctan\left(\frac{v_\beta^* - Ri_\beta}{v_\alpha^* - Ri_\alpha}\right) - \frac{V}{E}\omega_e T - \arctan\left(\frac{\lambda_{PM}}{L_q i_q}\right) \quad (3.25)$$

where v_α^* and v_β^* are the reference voltages and V , E and T are the RMS voltages, the back-EMF and the lag time caused by the inverter respectively. This estimator was robust and showed great dynamic performance at the experimental results.

For IPMSMs the mathematical model in the d - q rotating frame gets complicated because of its saliency and two trigonometric function of 2θ appears. The reason of this is the asymmetric impedance matrix, which can be rewritten symmetrically; in this way we get the extended EMF. Based on [1] the EEMF in the α - β stationary frame can be written as

$$\begin{aligned} \begin{bmatrix} v_\alpha \\ v_\beta \end{bmatrix} &= \begin{bmatrix} R_s + \frac{d}{dt}L_d & \omega_e(L_d - L_q) \\ -\omega_e(L_d - L_q) & R_s + \frac{d}{dt}L_d \end{bmatrix} \begin{bmatrix} i_\alpha \\ i_\beta \end{bmatrix} + \dots \\ &\dots + \{(L_d - L_q)\left(\omega_e i_d - \frac{d}{dt}i_q\right) + \omega_e \psi_M\} \begin{bmatrix} -\sin(\theta_e) \\ \cos(\theta_e) \end{bmatrix}. \end{aligned} \quad (3.26)$$

As the second term is the back-EMF vector, from this equation the position of the rotor can be extracted easily using eq. 3.27.

$$\theta_e = \arctan\left(\frac{-e_\alpha}{e_\beta}\right) \quad (3.27)$$

3.3.2 Adaptive methods

In the previous section it was presented that nonadaptive methods are an easy way to estimate the position of PMSM machines, but it could also be seen that mostly they are not robust enough and way too sensitive for the parameters. These methods used only some measured values of the system and the estimated position was calculated based on the model, but there was no feedback how punctual our calculations were. To improve robustness adaptive methods started to appear.

When the mathematical model of the electric drive is known, some outputs of the machine can be estimated or calculated. Adaptive methods use these estimated outputs and compare to the measured ones. The aim is to minimize the error between the measured and the calculated output by adapt the parameters of the model.

The adaptive methods usually use the following state-space equations as the model of the machine:

$$\begin{aligned}\underline{\dot{x}} &= \mathbf{A}\underline{x} + \mathbf{B}\underline{u} \\ \underline{y} &= \mathbf{C}\underline{x}\end{aligned}\tag{3.28}$$

3.3.2.1 Estimator based on Model Reference Adaptive System (MRAS)

The MRAS method consists two models, the Reference Model (RM) and the Adaptive Model (AM). The RM is the desired mathematical model of the machine and can be described with eq. 3.28. The AM contains an additional part which is the difference between the output of the two models. The equations of the AM is the following:

$$\begin{aligned}\underline{\dot{\hat{x}}} &= \hat{\mathbf{A}}\underline{\hat{x}} + \mathbf{B}\underline{u} + \mathbf{K}(\underline{y} - \underline{\hat{y}}) \\ \underline{\hat{y}} &= \mathbf{C}\underline{\hat{x}}\end{aligned}\tag{3.29}$$

where x is the state vector, u is the input vector, y is the output vector and \mathbf{A} , \mathbf{B} and \mathbf{C} matrices are the parameters of the machine, while matrix \mathbf{K} is a gain coefficient. The $\hat{}$ symbol denotes that the value of the term is estimated. An example system is presented on figure 3.2.

An error (ε) signal can be produced by the difference between the output of the RM and the AM. Using this the dynamic error equation can be written as [2]

$$\frac{d\varepsilon}{dt} = \frac{d}{dt}(\underline{x} - \underline{\hat{x}}) = (\mathbf{A} - \mathbf{K}\mathbf{C})\underline{\varepsilon} + (\mathbf{A} - \hat{\mathbf{A}})\underline{\hat{x}}.\tag{3.30}$$

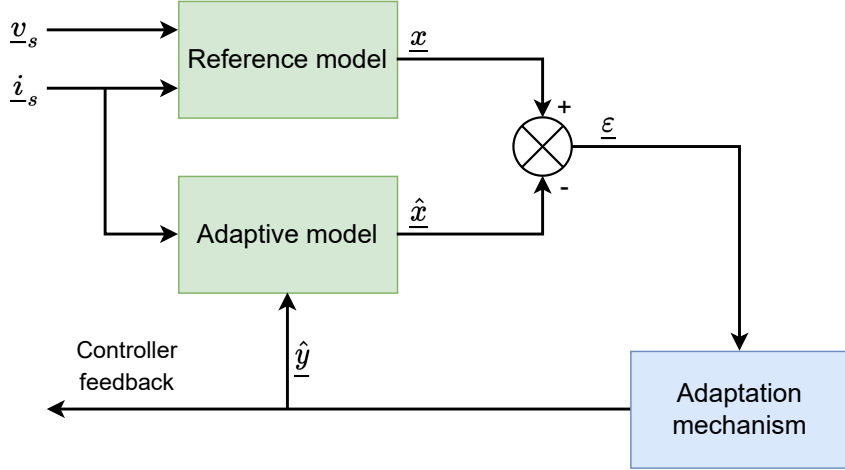


Figure 3.2: Block diagram of MRAS.

The estimated state variable can be either the rotor flux or the back-EMF. If the values of the K gain matrix are chosen properly, the AM becomes stable and the estimated state variables can be used for position and speed estimation. A possible adaptation mechanism can be the following

$$\hat{y} = K_P(x_q\hat{x}_d - \hat{x}_q x_d) + K_I \int_0^T (x_q\hat{x}_d - \hat{x}_q x_d) dt \quad (3.31)$$

where K_P and K_I are proportional and integral gains and x_d and x_q are the states of the machine in the d and q axis coordinates respectively [2].

3.3.2.2 Observer-based estimators

The basic idea of observers is the same as MRAS but instead of the reference model the real motor is used. The observer can be matched the adaptive model, where the gain matrix needs to be chosen in a way that the system is stable.

For a linear and deterministic plant the Luenberger observer can be used, while in non-deterministic cases the stochastic Kalman filter is the suitable solution. In case of nonlinear plants the extended Luenberger observer or the extended Kalman filter can be used [2].

Luenberger Observer

When using a Luenberger observer the model of the motor can be described with eq. 3.28. The model usually written in the α - β stationary reference frame, the state space variables are the currents and the back-EMF values.

The back-EMF in the stationary frame can be expressed as

$$\underline{e} = \begin{bmatrix} e_\alpha \\ e_\beta \end{bmatrix} = \{(L_d - L_q)(\omega_e i_d - \frac{d}{dt} i_q) + \omega_e \psi_M\} \begin{bmatrix} -\sin(\theta_e) \\ \cos(\theta_e) \end{bmatrix}. \quad (3.32)$$

The state space model of the machine can be written as

$$\begin{aligned} \frac{d}{dt} \begin{bmatrix} \dot{i}_{\alpha\beta} \\ \underline{e}_{\alpha\beta} \end{bmatrix} &= \mathbf{A} \begin{bmatrix} \dot{i}_{\alpha\beta} \\ \underline{e}_{\alpha\beta} \end{bmatrix} + \mathbf{B} \underline{u}_{\alpha\beta} + \mathbf{W} \\ \dot{i}_{\alpha\beta} &= \mathbf{C} \begin{bmatrix} \dot{i}_{\alpha\beta} \\ \underline{e}_{\alpha\beta} \end{bmatrix} \end{aligned} \quad (3.33)$$

where \mathbf{A} , \mathbf{B} , \mathbf{C} are matrices based on the motor model, \mathbf{W} is the unknown linearization error which could be neglected during the design of the observer, and

$$\begin{aligned} \dot{i}_{\alpha\beta s} &= [i_{\alpha s} \quad i_{\beta s}]^T \\ \underline{e}_{\alpha\beta s} &= [e_{\alpha s} \quad e_{\beta s}]^T. \end{aligned}$$

Similarly to the MRAS, the state space equation of the observer is almost the same as the machine's model, but consists an additional gain matrix to eliminate the error between the measured and the estimated currents.

$$\begin{aligned} \frac{d}{dt} \begin{bmatrix} \hat{\dot{i}}_{\alpha\beta} \\ \hat{\underline{e}}_{\alpha\beta} \end{bmatrix} &= \hat{\mathbf{A}} \begin{bmatrix} \hat{\dot{i}}_{\alpha\beta} \\ \hat{\underline{e}}_{\alpha\beta} \end{bmatrix} + \mathbf{B} \underline{u}_{\alpha\beta} + \mathbf{L}(\dot{i}_{\alpha\beta} - \hat{\dot{i}}_{\alpha\beta}) \\ \hat{\dot{i}}_{\alpha\beta} &= \mathbf{C} \begin{bmatrix} \hat{\dot{i}}_{\alpha\beta} \\ \hat{\underline{e}}_{\alpha\beta} \end{bmatrix} \end{aligned} \quad (3.34)$$

If the error of the currents is 0, then the estimated back-EMF values can be used for determining the speed and the position. It should be noted that the equation is dependent on ω_e which means the observer gains are different at different speeds. At implementation this could be handled eg. via a look-up table. The parameters of the state space equation and the observer design won't be presented in detail here, as it will be shown in chapter 4.

The estimated speed and position can be calculated several ways, the easiest one is the usage of a PI controller like tracking loop. The input of the tracking loop can be an error formed from the estimated back-EMF values, and the K_P and K_I gains can determine the dynamics of the estimation process.

In [24] a more complex PII structure was proposed instead of the regular PI one in order to compensate the estimation error during the transient state. The second

integral term uses the double integral of current change so that gives a boost to the corrector mechanism when fast changes happen in the system.

In [2] several other estimator schemes were shown. One of the methods used the actual rotor speed and the product of the i_d and i_q currents, instead of the back-EMF vectors in the state space model. It is also stated if a salient linear observer is used instead of the non-salient one, then 40% improvement can be achieved in the position estimation error. When using more complex estimator structures parameter tuning can become difficult. Proper parameter tuning can be done via doing parameter sweep or using novel solutions, eg. Genetic Algorithms (GA).

Using Luenberger observer can be a compromise solution among adaptive methods as it has better performance and more robust than the MRAS-based systems but computationally less demanding than the use of Kalman filter.

Reduced Order Observer

As in the aforementioned methods, the basic of the reduced order observer is a state space model in the form given by eq. 3.28, where (\mathbf{C}, \mathbf{A}) is observable. The reduced order observer design method is proposed in [5]. The paper states that if the y output vector can be written as a combination of the state vectors as

$$y = \mathbf{C}_1 x_1 + \mathbf{C}_2 x_2, \quad \det(\mathbf{C}_2) \neq 0 \quad (3.35)$$

then, it is sufficient to design an observer only for the partial state x_1 . If \hat{x}_1 is the estimation of x_1 , then x_2 can be estimated with the following.

$$\hat{x}_2 = \mathbf{C}_2^{-1}(y - \mathbf{C}_1 \hat{x}_1) \quad (3.36)$$

To design the reduced order observer the original system needs to be transformed to the following form

$$\begin{aligned} \dot{x}_1 &= \mathbf{A}_{11}x_1 + \mathbf{A}_{12}y + \mathbf{B}_1u \\ \dot{y} &= \mathbf{A}_{21}x_1 + \mathbf{A}_{22}y + \mathbf{B}_2u \end{aligned} \quad (3.37)$$

and a new variable x' can be constructed as

$$x' = x_1 + \mathbf{L}_1 y \quad (3.38)$$

where \mathbf{L}_1 is a nonsingular gain matrix. After substituting eq. 3.37 in eq. 3.38 and differentiating to x' the following term is obtained.

$$\dot{x}' = (\mathbf{A}_{11} + \mathbf{L}_1\mathbf{A}_{21})x' + (\mathbf{A}_{12} + \mathbf{L}_1\mathbf{A}_{22} - \mathbf{A}_{11}\mathbf{L}_1 - \mathbf{L}_1\mathbf{A}_{21}\mathbf{L}_1)y + (\mathbf{B}_1 + \mathbf{L}_1\mathbf{B}_2)u \quad (3.39)$$

For x' an observer can be designed using the following form.

$$\dot{\hat{x}}' = (\mathbf{A}_{11} + \mathbf{L}_1\mathbf{A}_{21})\hat{x}' + (\mathbf{A}_{12} + \mathbf{L}_1\mathbf{A}_{22} - \mathbf{A}_{11}\mathbf{L}_1 - \mathbf{L}_1\mathbf{A}_{21}\mathbf{L}_1)y + (\mathbf{B}_1 + \mathbf{L}_1\mathbf{B}_2)u \quad (3.40)$$

From these, the error dynamics of the system can be described as

$$\dot{\bar{x}} = (\mathbf{A}_{11} + \mathbf{L}_1\mathbf{A}_{21})\bar{x}'. \quad (3.41)$$

If \mathbf{A}_{11} and \mathbf{A}_{21} are known, the gains of \mathbf{L}_1 can be designed on a way that the error tends to zero. When \hat{x}' is estimated, the value of x_1 and x_2 can be calculated using eq. 3.38 and eq. 3.36.

In [5] it is presented that the reduce order observer is suitable to estimate both the stator flux or the EMF. Any of them is eligible to estimate the speed and position values and to control the system.

Sliding Mode Observer (SMO)

The sliding mode observer is really similar to the Luenberger observer, the main difference is the calculation of the error. While in the Luenberger observer the difference between the estimated and the measured value is the error function, in SMO only the sign-function of the difference is used. The scheme of the observer can be described as

$$\begin{aligned} \dot{\hat{x}} &= \mathbf{A}\hat{x} + \mathbf{B}u + \mathbf{K} \cdot \text{sgn}(y - \hat{y}) \\ \hat{y} &= \mathbf{C}\hat{x} \end{aligned} \quad (3.42)$$

In [27] an improved method called adaptive SMO is proposed, which combines the regular observer scheme with the SMO. A new Φ gain is also inserted into the system, which can be described with the following set of equations.

$$\begin{aligned} \dot{\hat{x}} &= \mathbf{A}\hat{x} + \mathbf{B}u + \mathbf{K}(y - \hat{y}) + \Phi \cdot \text{sgn}(y - \hat{y}) \\ \hat{y} &= \mathbf{C}\hat{x} \end{aligned} \quad (3.43)$$

3.3.2.3 Kalman Filter and Extended Kalman Filter (EKF)

The regular Kalman filters can be used on linear systems. Based on [2] the IPMSM can be described with the following equations

$$\begin{aligned}\dot{\underline{x}} &= \mathbf{A}\underline{x} + \mathbf{B}\underline{u} + \underline{v} \\ \underline{y} &= \mathbf{C}\underline{x} + \underline{n}\end{aligned}\quad (3.44)$$

where \underline{v} is the system- and \underline{n} is the measuring disturbance, which has a white noise character. The state space equation of the Kalman filter is the same as the Luenberger observer, the difference between the methods is the selection of the observer gain matrix.

The variance of \underline{v} and \underline{n} are given as [2]

$$\begin{aligned}E\{\underline{v} \cdot \underline{v}^T\} &= \mathbf{Q} \cdot \delta(t - \tau) \quad (\mathbf{Q} \text{ positive semidefinite}) \\ E\{\underline{n} \cdot \underline{n}^T\} &= \mathbf{R} \cdot \delta(t - \tau) \quad (\mathbf{R} \text{ positive definite})\end{aligned}\quad (3.45)$$

where \mathbf{Q} and \mathbf{R} are covariance matrices. The dynamics of error ε can be expressed as

$$\dot{\underline{\varepsilon}} = (\mathbf{A} - \mathbf{K}\mathbf{C})\underline{\varepsilon} + \underline{v} - \mathbf{K}\underline{n}. \quad (3.46)$$

To ensure the the optimum state estimation \mathbf{K} must be selected properly. This can be done via using the following form

$$\mathbf{K} = \mathbf{P}\mathbf{C}^T\mathbf{R}^{-1} \quad (3.47)$$

where \mathbf{P} is the solution of the Riccati differential equation, given by eq. 3.48 with the initial value $\mathbf{P}(0)$ [2].

$$\dot{\mathbf{P}} = \mathbf{A}\mathbf{P} + \mathbf{P}\mathbf{A}^T + \mathbf{Q} - \mathbf{P}\mathbf{C}^T\mathbf{R}^{-1}\mathbf{C}\mathbf{P} \quad \text{where} \quad \mathbf{P}(0) = E\{\underline{\varepsilon}(0) \cdot \underline{\varepsilon}^T(0)\} \quad (3.48)$$

In [2] it is mentioned, that the most difficult part of designing the Kalman filter is the selection of $\mathbf{P}(0)$, \mathbf{Q} and \mathbf{R} matrices.

In case of nonlinear systems the extended Kalman filter (EKF) can be used. This type of filter solves the problem of nonlinearity by linearizing the recently estimated state [14]. The estimation process of a discretized EKF consists of 3 steps: the forecasting phase, the revision phase and the update of the Kalman gain. In [14] a solution is mentioned also, where the 2-phase stationary voltages and currents were

taken as the inputs and outputs of the system, while the stator flux, the rotor speed and the position were used as state variables.

The drawback of the EKF method is the calculation workload, hence it can not be used on cheaper microcontrollers as it is computationally demanding.

3.4 Artificial Intelligence based methods

In [14] a review of artificial intelligence based methods is presented. Mostly artificial neural networks (ANN) are used in sensorless control. A regular neural network consists of multiple layers: an input layer, one or more hidden layers and an output layer. The neural networks can be grouped in two main categories, the feedforward NN and the feedback NN. Based on [14] the neural networks can be grouped as:

- Feedforward neural network
 - Perceptron
 - Multi-layer perceptron
 - * Error back propagation neural network (BP-NN)
 - * Radial basis function neural network (RBF-NN)
 - * Support vector machines (SVM)
 - Deep learning
 - * Deep neural network (DNN)
 - * Deep belief network (DBN)
 - * Convolutional neural network (CNN)
- Feedback neural network
 - Hopfield NN
 - Elman NN
 - Boltzmann machine
 - Wavelet NN

Usually ANNs are used for connecting the voltage, current and rotor position of the measured phase through adaptive technology [14]. The paper also presents a basic state equation in the α - β frame that can be used by the NN, it is given in the following form

$$\hat{x} = \mathbf{A}x + f(x, u)$$

$$y = \mathbf{C}x + v \quad (3.49)$$

where

$$x = \begin{bmatrix} x_1 \\ x_2 \end{bmatrix} = \begin{bmatrix} \frac{\psi_M}{L} \omega_e \sin \theta_e \\ -\frac{\psi_M}{L} \omega_e \cos \theta_e \end{bmatrix}, \quad u = \begin{bmatrix} i_\alpha \\ i_\beta \end{bmatrix}, \quad y = \begin{bmatrix} \hat{i}_\alpha \\ \hat{i}_\beta \end{bmatrix}. \quad (3.50)$$

Chapter 4

A proposed wide-speed-range sensorless control method

In this chapter a combination of sensorless methods will be presented that could estimate the rotor position and speed of PMSMs at both low, middle and high-speeds. Firstly, a zero speed initial position estimator will be introduced, then a low-speed and then a medium and high-speed method will be presented. Finally it will be discussed how the switching between the later two methods can happen during transient operation. This chapter mainly focuses on the theory, as the design and the practical usage will be stated in chapter 5 in detail.

4.1 Initial position estimation: DC pulse injection

If we want to use different sensorless control methods, we must know the initial rotor position accurately to make correct predictions. DC pulse injection can be used for this purpose in case of a PMSM with structural saliency (L_d and L_q values are different). It is important to note that DC pulse injection technique does not work on SPMSMs. The method has been used for a long time and it is discussed in detail in several papers [19, 28, 26]. The procedure consists of two easy steps.

Firstly, a low voltage short DC pulse is used to determine the rotor's orientation which tells us only the orientation of the d - q axes but not their direction [12]. The pulses should be injected in all three phases which indicates current that can be measured. We use a positive and a negative impulse just after each other to increase the phase current and decrease it back to 0 immediately. This is repeated in the

negative direction also. It is important to hold a short time delay before applying the next pulse pair, in order to let all phase currents reset to 0 properly. The orientation can be calculated from the measured peak values.

The d axis is closest to the phase in which the peak current is the largest, because PMSMs have larger inductance in the q direction. From this information we know the angle of the d axis in a ± 30 degrees range. The accurate offset can be calculated using the other 2 phases' peak currents as the following [26]

$$\theta_{offset} = \frac{\cos(120^\circ) I_1 - I_2}{\sin(120^\circ) I_1 + I_2} \quad (4.1)$$

where I_1 and I_2 are the differences between the maximum and minimum peak in the other 2 phases.

Secondly a high voltage pulse is applied to the d axis to identify the rotor's polarity. By applying the pulse accurately to the d axis, the movement of the rotor is minimized. The direction of the d axis is determined by the difference of a positive and a negative pulse, because the north and south poles of the rotor magnets saturate the stator coils differently.

4.2 Low-speed control: High frequency alternating signal injection

As BEMF signal is insufficient at lower speeds and standstill, state observers which use BEMF for speed and position estimation can't be used in low-speed range. A possible solution for this problem is the use of different signal injection techniques. At high frequency ranges a high frequency PMSM model can be used, which can be obtained by transforming the elements of eq. 2.9 to high frequency terms and based on [10] it can be written in the following form

$$\begin{aligned} \begin{bmatrix} v_{dsh}^r \\ v_{qsh}^r \end{bmatrix} &= \begin{bmatrix} r_{dh}^r + \frac{d}{dt} L_{dh}^r & 0 \\ 0 & r_{qh}^r + \frac{d}{dt} L_{qh}^r \end{bmatrix} \begin{bmatrix} i_{dsh}^r \\ i_{qsh}^r \end{bmatrix} \\ &= \begin{bmatrix} r_{dh}^r + j\omega L_{dh}^r & 0 \\ 0 & r_{qh}^r + j\omega L_{qh}^r \end{bmatrix} \begin{bmatrix} i_{dsh}^r \\ i_{qsh}^r \end{bmatrix} = \begin{bmatrix} z_{dh}^r & 0 \\ 0 & z_{qh}^r \end{bmatrix} \begin{bmatrix} i_{dsh}^r \\ i_{qsh}^r \end{bmatrix} \end{aligned} \quad (4.2)$$

where z_{dh}^r and z_{qh}^r are the d and q axes high frequency impedances in the actual rotor reference frame. As the actual rotor position is not available in sensorless operation,

we need to use the estimated rotor reference frame later in our calculations. The position estimation error can be written as

$$\tilde{\theta}_e = \theta_e - \hat{\theta}_e \quad (4.3)$$

where θ_e is the actual electrical rotor position and $\hat{\theta}_e$ is the estimated rotor position. Based on [10] the model in estimated rotor reference frame can be continued as

$$\begin{aligned} \begin{bmatrix} v_{dsh}^{\hat{r}} \\ v_{qsh}^{\hat{r}} \end{bmatrix} &= R(\tilde{\theta}_e)^{-1} \begin{bmatrix} z_{dh}^r & 0 \\ 0 & z_{qh}^r \end{bmatrix} R(\tilde{\theta}_e) \begin{bmatrix} i_{dsh}^{\hat{r}} \\ i_{qsh}^{\hat{r}} \end{bmatrix} \\ &= \begin{bmatrix} z_{avg} + \frac{z_{diff}}{2} \cos(2\tilde{\theta}_e) & \frac{z_{diff}}{2} \sin(2\tilde{\theta}_e) \\ \frac{z_{diff}}{2} \sin(2\tilde{\theta}_e) & z_{avg} - \frac{z_{diff}}{2} \cos(2\tilde{\theta}_e) \end{bmatrix} \begin{bmatrix} i_{dsh}^{\hat{r}} \\ i_{qsh}^{\hat{r}} \end{bmatrix} \end{aligned} \quad (4.4)$$

where

$$\begin{aligned} R(\theta) &= \begin{bmatrix} \cos(\theta) & \sin(\theta) \\ -\sin(\theta) & \cos(\theta) \end{bmatrix} \\ z_{avg} &= \frac{z_{dh}^r + z_{qh}^r}{2} \\ z_{diff} &= z_{dh}^r - z_{qh}^r. \end{aligned}$$

The final formula for the model in the estimated rotor reference frame is the following

$$\begin{bmatrix} v_{dsh}^{\hat{r}} \\ v_{qsh}^{\hat{r}} \end{bmatrix} = \begin{bmatrix} z_{dh}^{\hat{r}} & z_{ch}^{\hat{r}} \\ z_{ch}^{\hat{r}} & z_{qh}^{\hat{r}} \end{bmatrix} \begin{bmatrix} i_{dsh}^{\hat{r}} \\ i_{qsh}^{\hat{r}} \end{bmatrix} \quad (4.5)$$

where $z_{dh}^{\hat{r}}$, $z_{qh}^{\hat{r}}$ and $z_{ch}^{\hat{r}}$ are the d axis, q axis and cross-coupling high frequency impedances [10]. We should notice that even though the actual rotor reference frame model has no cross-coupling impedances, when the estimated rotor reference frame is used these impedances also need to be used.

From the previous equations we get the following terms

$$\begin{aligned} z_{dh}^{\hat{r}} &= z_{avg} + \frac{1}{2} z_{diff} \cos(2\tilde{\theta}_e) \\ z_{qh}^{\hat{r}} &= z_{avg} - \frac{1}{2} z_{diff} \cos(2\tilde{\theta}_e) \\ z_{ch}^{\hat{r}} &= \frac{1}{2} z_{diff} \sin(2\tilde{\theta}_e). \end{aligned} \quad (4.6)$$

For the injection we have two options, either the alternating signal is injected only on the d axis, or on the q axis. Injecting signals only on the d axis is better, as it

won't produce torque ripples. The injected signal can be written as

$$\begin{bmatrix} v_{dsh}^{\hat{r}} \\ v_{qsh}^{\hat{r}} \end{bmatrix} = \begin{bmatrix} V_{inj} \cos(\omega_h t) \\ 0 \end{bmatrix}. \quad (4.7)$$

If high frequency inductances are much larger than the resistances the relation between i_q and the error of θ_e will be the following [10]

$$i_{qsh}^{\hat{r}} = -\frac{z_{ch}^{\hat{r}}}{z_{dh}^{\hat{r}} z_{qh}^{\hat{r}}} V_{inj} \cos(\omega_h t) \approx \left[\frac{V_{inj} r_{diff} \cos(\omega_h t)}{2 \omega_h^2 L_{dh}^r L_{qh}^r} - \frac{\omega_h L_{diff} \sin(\omega_h t)}{\omega_h^2 L_{dh}^r L_{qh}^r} \right] \sin(2\tilde{\theta}_e). \quad (4.8)$$

From this estimated current the rotor position estimation can be extracted by using a band-pass filter, a multiplication and a low-pass filter.

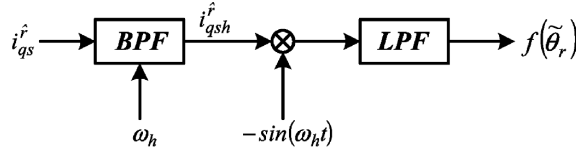


Figure 4.1: Signal processing for the high frequency signal injection method [10].

After the signal processing, the rotor position estimation error approximately can be described with the following term.

$$f(\tilde{\theta}_e) \approx \frac{V_{inj} L_{diff}}{2\omega_h L_{dh}^r L_{qh}^r} \tilde{\theta}_e = K_{err} \tilde{\theta}_e \quad (4.9)$$

As the estimated rotor position error is produced, the speed can be approximated via using a PI tracking loop. To express the current rotor position the estimated speed should be integrated. An example of the full control loop is shown on figure 4.2.

It must be noted, that the limitation of high frequency AC injection is when the L_d and L_q inductances are equal or close to each other [21]. It can be seen also from eq. 4.9 where the L_{diff} term appears in the numerator, which becomes zero when $L_{dh}^r = L_{qh}^r$. It also means the position error is zero independently any other values.

4.3 High-speed control: Luenberger observer

A Luenberger observer can be used for estimating the internal state of a system by measuring only its inputs and outputs. A simple block diagram of the observer is

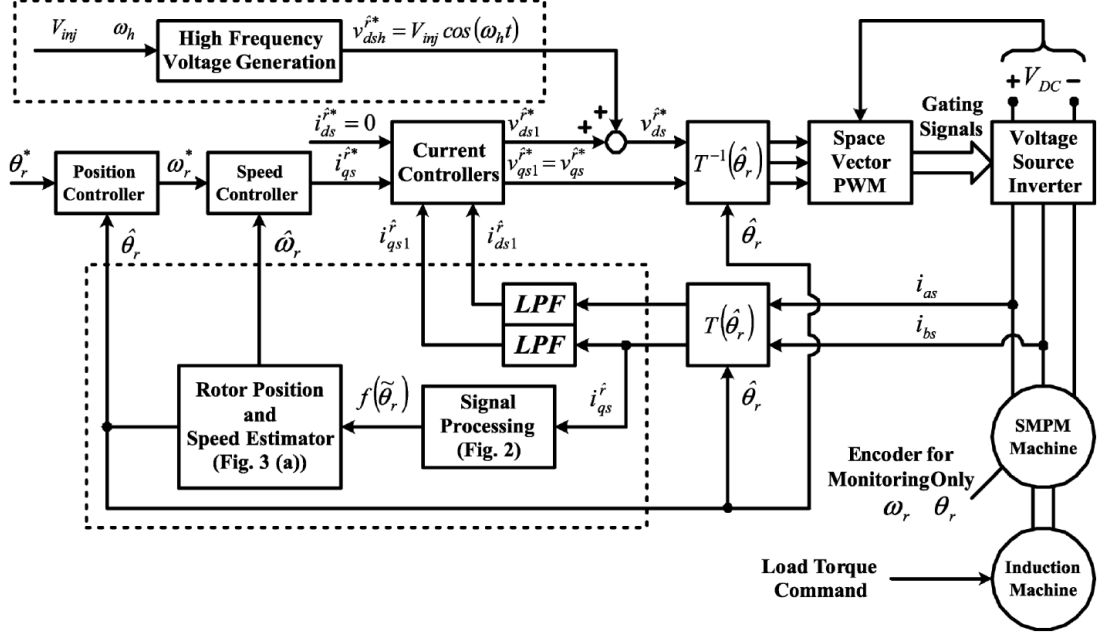


Figure 4.2: An example control loop for the high frequency injection method [10].

shown on figure 4.3. In our case the BEMF of the PMSM is estimated by measuring the stator phase currents and the voltages applied to the stator windings. The speed and position can be determined from the estimated BEMF by using a tracking loop.

4.3.1 State space model of the observer

A general state space model of a system looks the following.

$$\begin{aligned}\dot{\underline{x}} &= \mathbf{A}\underline{x} + \mathbf{B}\underline{u} \\ \underline{y} &= \mathbf{C}\underline{x}\end{aligned}\quad (4.10)$$

The \mathbf{A} , \mathbf{B} and \mathbf{C} matrices should be determined based on the real PMSM machine, either more complex or simplified models also can be used.

The form of the BEMF vector can be written as eq. 4.11 if the α - β stationary frame is used and the electrical system's time constant is much smaller than the mechanical one [2, 16].

$$\underline{e} = \begin{bmatrix} e_\alpha \\ e_\beta \end{bmatrix} = \{(L_d - L_q)(\omega_e i_d - \frac{d}{dt} i_q) + \omega_e \psi_M\} \begin{bmatrix} -\sin(\theta_e) \\ \cos(\theta_e) \end{bmatrix}\quad (4.11)$$

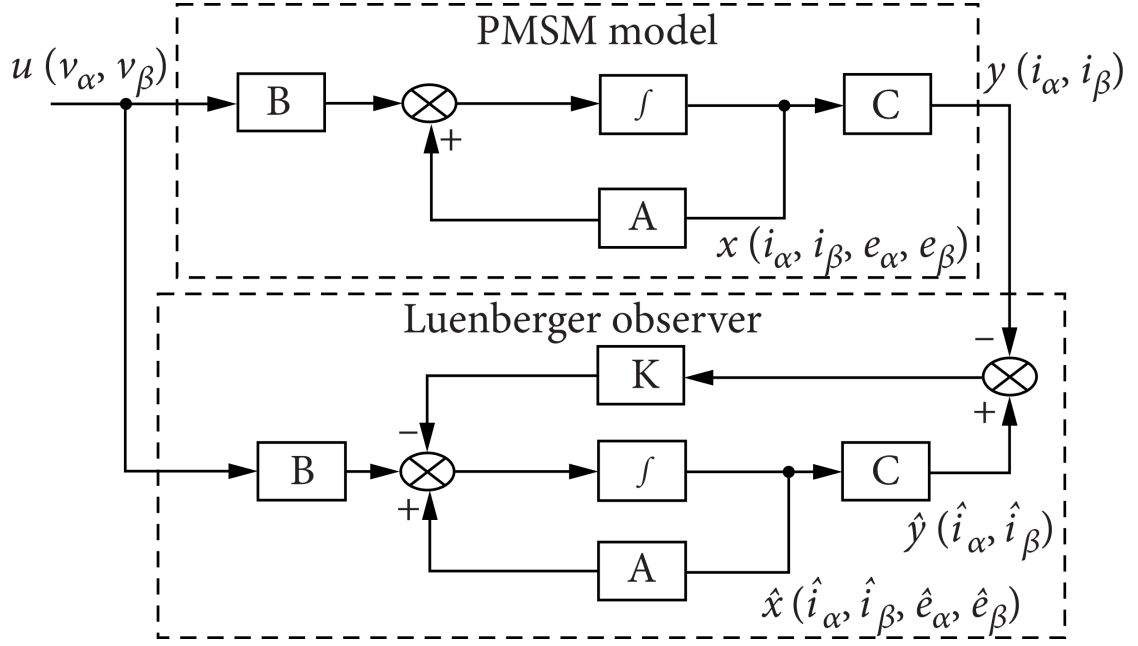


Figure 4.3: Block diagram of the Luenberger observer for PMSMs, where \mathbf{K} stands for the observer gain [15].

Based on the aforementioned formulas the state equation for PMSMs can be described as [2, 16]

$$\begin{aligned} \frac{d}{dt} \begin{bmatrix} \dot{i}_{\alpha\beta} \\ \underline{e}_{\alpha\beta} \end{bmatrix} &= \mathbf{A} \begin{bmatrix} \dot{i}_{\alpha\beta} \\ \underline{e}_{\alpha\beta} \end{bmatrix} + \mathbf{B}v_{\alpha\beta} + \mathbf{W} \\ \dot{i}_{\alpha\beta} &= \mathbf{C} \begin{bmatrix} \dot{i}_{\alpha\beta} \\ \underline{e}_{\alpha\beta} \end{bmatrix} \end{aligned} \quad (4.12)$$

where the state variables are

$$\begin{aligned} \dot{i}_{\alpha\beta} &= [i_{\alpha} \quad i_{\beta}]^T \\ \underline{e}_{\alpha\beta} &= [e_{\alpha} \quad e_{\beta}]^T \end{aligned}$$

and, based on [4, 9], the matrices can be obtained as

$$\mathbf{A} = \begin{bmatrix} \frac{-R_s}{L_d} & \frac{-\omega_e(L_d-L_q)}{L_d} & \frac{-1}{L_d} & 0 \\ \frac{\omega_e(L_d-L_q)}{L_d} & \frac{-R_s}{L_d} & 0 & \frac{-1}{L_d} \\ 0 & 0 & 0 & -\omega_e \\ 0 & 0 & \omega_e & 0 \end{bmatrix}$$

$$\mathbf{B} = \frac{1}{L_d} \begin{bmatrix} 1 & 0 \\ 0 & 1 \\ 0 & 0 \\ 0 & 0 \end{bmatrix}, \quad \mathbf{C} = \begin{bmatrix} 1 & 0 & 0 & 0 \\ 0 & 1 & 0 & 0 \end{bmatrix}$$

$$\mathbf{W} = (L_d - L_q)(\omega_e i_d - i_q) \begin{bmatrix} -\sin(\theta) \\ \cos(\theta) \end{bmatrix}.$$

When i_d and i_q is changing there is an unknown linearization error in the system (that's what \mathbf{W} stands for), but at observer design and in practise this effect is negligible.

In this formula ω_e is a constant parameter, hence we need to calculate with the actual electrical angular frequency in our model. This means, the observer parameters varying by the rotor speed, so the observer parameters can be determined on specific ω_e values. This can be done by using a look-up-table during operation.

The state equation for the Luenberger observer is very similar to the system's state space model and can be written as the following [2].

$$\begin{aligned} \frac{d}{dt} \begin{bmatrix} \hat{i}_{\alpha\beta} \\ \hat{e}_{\alpha\beta} \end{bmatrix} &= \hat{\mathbf{A}} \begin{bmatrix} \hat{i}_{\alpha\beta} \\ \hat{e}_{\alpha\beta} \end{bmatrix} + \mathbf{B}v_{\alpha\beta} + \mathbf{L}(i_{\alpha\beta} - \hat{i}_{\alpha\beta}) \\ \hat{i}_{\alpha\beta} &= \mathbf{C} \begin{bmatrix} \hat{i}_{\alpha\beta} \\ \hat{e}_{\alpha\beta} \end{bmatrix} \end{aligned} \quad (4.13)$$

As $\hat{\mathbf{A}}$ includes ω_e , the actual rotor speed should be estimated during operation. At observer design the \mathbf{L} matrix needs to be determined for different speed values, and during simulation the proper observer matrices must be chosen to the corresponding speed via a look-up-table.

If we want to simplify our model, we can assume that $L_d = L_q = L_s$, and the dependency of ω_e can be neglected. This results that the \mathbf{A} matrix does not contain ω_e at all and the observer parameters are constants. The simplified model and the corresponding observer design steps can be found in [23]. The article states that if the calculation steps are small enough, it can be assumed that the derivatives of BEMF signals are zero, thus at one calculation step the BEMF is constant. The matrices of the state space model, after the simplifications were made, can be written as

$$\mathbf{A} = \begin{bmatrix} -\frac{R_s}{L_s} & 0 & -\frac{1}{L_s} & 0 \\ 0 & -\frac{R_s}{L_s} & 0 & -\frac{1}{L_s} \\ 0 & 0 & 0 & 0 \\ 0 & 0 & 0 & 0 \end{bmatrix}, \quad \mathbf{B} = \frac{1}{L_s} \begin{bmatrix} 1 & 0 \\ 0 & 1 \\ 0 & 0 \\ 0 & 0 \end{bmatrix}, \quad \mathbf{C} = \begin{bmatrix} 1 & 0 & 0 & 0 \\ 0 & 1 & 0 & 0 \end{bmatrix}.$$

4.3.2 Observer design

Either the more complex or the simpler model is used, the observation can be calculated as the following [2, 16].

$$\hat{\underline{x}} = \mathbf{A}\hat{\underline{x}} + \mathbf{B}\underline{u} + \mathbf{L}(\underline{y} - \mathbf{C}\hat{\underline{x}}) = (\mathbf{A} - \mathbf{L}\mathbf{C})\hat{\underline{x}} + \mathbf{B}\underline{u} + \mathbf{L}\underline{y} \quad (4.14)$$

The observer parameters should be determined in a way that the observer will be stable during operation. The observer gain matrix \mathbf{L} can be calculated with Matlab's *acker* function in case of a SISO (single-input single-output) system. For MIMO (multiple-input multiple-output) systems \mathbf{L} can be determined by solving an equation for the characteristic polynomial of $\mathbf{A} - \mathbf{L}\mathbf{C}$. This calculation can be done via the following equation

$$\det(s\mathbf{I} - (\mathbf{A} - \mathbf{L}\mathbf{C})) = (s - p)^4 \quad (4.15)$$

where on the left side there is the characteristic polynomial, aka the eigenvalues of $(\mathbf{A} - \mathbf{L}\mathbf{C})$, while on the right side 4 poles can be found. These poles are need to be placed during observer design by choosing the value of p . The dynamics of the system is described by the characteristic polynomial. If a \mathbf{L} matrix is chosen, where $(\mathbf{A} - \mathbf{L}\mathbf{C})^T$ is negative semi-definite, then the speed observer will be stable [12].

4.3.3 Discretized Luenberger observer

In the previous sections all the models and equations were in continuous time, but the simulations and the implemented real system are sample based, hence a discretized observer can be constructed for better operation. If the sample time of the system is T_s , then the continuous time system can be discretized by using the forward Euler method, that can be written as

$$\mathbf{A}_{DI} = \mathbf{I} + \mathbf{A} \cdot T_s, \quad \mathbf{B}_{DI} = T_s \cdot \mathbf{B}, \quad \mathbf{C}_{DI} = \mathbf{C} \quad (4.16)$$

where \mathbf{A} , \mathbf{B} and \mathbf{C} are the system matrices of the continuous time model, while \mathbf{A}_{DI} , \mathbf{B}_{DI} and \mathbf{C}_{DI} are the matrices of the new discretized state space model. The new model can be written as

$$\begin{aligned}\underline{x}[k+1] &= \mathbf{A}_{DI}\underline{x}[k] + \mathbf{B}_{DI}u[k] \\ \underline{y}[k] &= \mathbf{C}_{DI}\underline{x}[k]\end{aligned}\quad (4.17)$$

where k indicates the k th time step. It can be seen from the state equation that the continuous time derivation is changed to a time delay, thus in the observer model shown on figure 4.3 the continuous integral also needs to be changed to a unit delay.

The design of the observer is the same for discrete time, the only difference is in the pole placement method. If p was chosen as a continuous time pole, then its discrete equivalent can be calculated with the $p_{DI} = e^{-pT_s}$ formula.

4.3.4 Extraction of rotor speed and position

The formerly presented observer is suitable to extract the BEMF values of the system, but from that the speed and position information still needs to be estimated. That can be done by using a PI controller-like tracking loop, which gets an error signal as input and produces the rotor speed as output. From the angular velocity the position can be obtained via using an integrator or it can be calculated from the back-EMF directly.

In [2] a possible PI controller is presented, using following formula

$$\hat{\omega}_e = K_P(\hat{e}_\alpha\varepsilon_\alpha - \hat{e}_\beta\varepsilon_\beta) + K_I \int (\hat{e}_\alpha\varepsilon_\alpha - \hat{e}_\beta\varepsilon_\beta) dt \quad (4.18)$$

where K_P and K_I are the gains of the controller, ε_α and ε_β are the current errors ($i - \hat{i}$) in the α - β reference frame.

Another possible solution is shown in [12], where the error signal is constructed from the current and the previous position. It can be written as

$$\begin{aligned}\hat{\omega}_e &= K_P\varepsilon + K_I \int \varepsilon dt \\ \varepsilon &= \sin(\hat{\theta}_e) \cdot \cos(\hat{\theta}'_e) - \cos(\hat{\theta}_e) \cdot \sin(\hat{\theta}'_e)\end{aligned}\quad (4.19)$$

where ε is the input error signal and $\hat{\theta}_e$ indicates the actual estimated electrical rotor position, while $\hat{\theta}'_e$ denotes the previous position.

4.4 Combining sensorless control methods

Different sensorless methods work better at different speeds, so multiple types of estimation required if we want to control the motor precisely at any speed. Previously I presented three methods for zero, low and high-speed control respectively.

The initial position estimation can happen at the beginning of the operation, so the zero speed estimation simply can be used after the process is completed. For the other two estimators, a switching logic is required in order to keep up the control, the whole speed range and make the estimation as precise as possible, even during transient states. At the implementation of the switching logic I will work based on [12], in which a speed interval is chosen, where the high-frequency signal injection and the Luenberger observer are both active, but contributes to the estimation with different weights.

It is mentioned in [12], if a more complex PMSM model is used the Luenberger observer should be accurate at higher speeds than the 10% of the nominal speed. In case of a simplified PMSM model the observer starts to get accurate around 30% of the nominal speed, hence the switching interval should be around this area. During the switching interval a linear transition can be used at the weights, to make the switch between the methods as smooth as possible.

Chapter 5

Simulation of sensorless methods

This chapter discusses how the simulation was prepared for testing the sensorless methods. Firstly some general information of the Simulink model will be provided, then the design of the regular FOC control loop will be presented, finally the simulation of the different sensorless estimator methods will be shown.

5.1 Overview of the simulation

5.1.1 Environment

For simulations the Matlab Simulink environment was used. In order to keep the Simulink model as simple as possible I tried to use mostly prepared items like controllers or Clarke and Park transform blocks. For the electrical part of the simulation the Simscape / Electrical / Specialized Power Systems library was used. As machine model firstly I used the Electrical Machines / Permanent Magnet Synchronous Machine component of the library, which can be used as a BLDC or as a PMSM drive. The model offers several settings, hence the electric machine can be parameterized according to our needs. Later it was changed to a model provided by my advisor, as the parameters of the original motor could not be changed during simulation, which is required for parameter sensitivity tests. The new model implements the mathematical equations of an IPMSM with basic Simulink blocks, hence the value of different parameters, like L_d and L_q inductances, can be changed during simulation. As a 3 phase inverter the Universal Bridge block was used where the power electronic device was set to MOSFET / Diodes. The library also includes current and voltage measurement sensors that were used in my simulation.

It is worth mentioning that the parameters of the simulation should be set carefully, because using Matlab's auto setting could distort the results of the simulation. In the Configuration Parameters / Solver tab it is advised to set the max step size at least an order of magnitude lower than the fastest components step time. Using the auto setting sometimes resulted small oscillations at the steady state of signals in which case I suspected a wrong parameter setting at the controller. After several tries it was found that the problem was not caused by an inappropriate parameter, but the solver's settings, since lowering the max step size resolved the issue.

5.1.2 Machine parameters

At the simulations the parameters of the electric drive are set almost identical to the machine that is used at implementation. The only difference is in the value of d and q -axis inductances, which are equal at the real machine, as it is a SPMSM. Even though preparing the simulations on different parameters is not optimal from the implementation point of view, but different L_d and L_q is required for some sensorless estimator methods.

This is not a problem at the Luenberger observer, because in this case SPMSMs can be regarded as a particular case of IPMSMs where $L_d = L_q$. As it was mentioned in section 4.2 the high-frequency signal injection is operable only if L_d and L_q are different, hence in case of SPMSMs the method might not work. This is the reason why at the simulations equal inductances can not be used.

Considering the aforementioned things, the machine parameters that were used in the simulation:

- Number of pole pairs: 5
- d and q axis inductances: $L_d = 0.21 \text{ mH}$ and $L_q = 0.43 \text{ mH}$
- Stator resistance: $R_s = 0.285 \Omega$
- Torque constant: $K_t = 0.05917 \frac{\text{Nm}}{\text{A}}$
- Inertia: $J = 7.77 \times 10^{-5} \text{ kg m}^2$
- Viscous damping: $F = 5 \times 10^{-5} \text{ Nms}$

The parameters of the inverter bridge:

- Nominal DC voltage: 24 V
- PWM switching frequency: $f_{PWM} = 10 \text{ kHz}$

5.1.3 Control loop without estimation

In order to test and compare the sensorless speed and position estimators a regular FOC control loop had to be designed, where the later estimated parameters are known. The system is a two level cascade control, where the outer loop is a PI speed controller and the inside loop is the current control of the d and q axis currents. After applying the inverse Park and Clarke transformations a three phase inverter produces the inputs of the PMSM block. The output of the machine contains all required data such as the actual speed and position of the motor and the three phase currents. After applying the regular Clarke and Park transformations the sampled current values can be fed back to the current controllers, while the sampled angular velocity is attached back to the speed controller.

The sample time of the control loops are:

- Current control: $T_s = 0.1 \text{ ms}$
- Speed control: $T_{s\omega} = 1 \text{ ms}$

The controller gains in the system were designed based on the machine parameters. The P and I values of the current controllers were calculated separately for the d and q axis because the L_d and L_q inductances are slightly different. The transfer function of the PI can be written as

$$PI_{id}(z) = K_{id} \left(1 + I_{id} T_s \frac{1}{z-1} \right) \quad \text{and} \quad PI_{iq}(z) = K_{iq} \left(1 + I_{iq} T_s \frac{1}{z-1} \right) \quad (5.1)$$

where id and iq denotes the d and the q axis values. K_i and I_i can be calculated as

$$\begin{aligned} K_{id} &= 0.5 \frac{L_d}{T_d} \quad \text{and} \quad T_{id} = \frac{L_d}{R_s} \quad \text{and} \quad I_{id} = \frac{1}{T_{id}} \\ K_{iq} &= 0.5 \frac{L_q}{T_d} \quad \text{and} \quad T_{iq} = \frac{L_q}{R_s} \quad \text{and} \quad I_{iq} = \frac{1}{T_{iq}} \end{aligned} \quad (5.2)$$

where L_d and L_q are the d and q axis inductances, $T_d = \frac{3}{2}T_s$ is the dead time of the system, while T_{id} and T_{iq} are the electrical time constants of the motor. In my simulation the numerical values of the constants are

$$\begin{aligned} K_{id} &= 0.7000 \quad \text{and} \quad T_{id} = 7.3684 \times 10^{-4} \text{ sec} \\ K_{iq} &= 1.4333 \quad \text{and} \quad T_{iq} = 1.5088 \times 10^{-3} \text{ sec}. \end{aligned}$$

As previously mentioned, the maximum torque can be achieved by controlling the i_d current with different techniques, like MTPA. For simplicity in my simulations i_d

was set to 0 constantly. Although this solution does not provide maximum torque at higher speeds, the control performance is still sufficient and it has no effect on the inspection of sensorless methods.

The transfer function of the speed controller is

$$PI_{\omega}(z) = K_{\omega} \left(1 + I_{\omega} T_{s\omega} \frac{1}{z-1} \right) \quad (5.3)$$

where K_{ω} and I_{ω} can be determined as

$$K_{\omega} = \frac{J}{K_t \omega_c}, \quad T_{\omega} = B T_{d\omega}, \quad \omega_c = \frac{1}{\sqrt{T_{\omega} T_d}} \quad \text{and} \quad I_{\omega} = \frac{1}{T_{\omega}} \quad (5.4)$$

where J is the motor inertia, K_t is the torque constant, ω_c is the cutoff frequency, B is a constant (chosen as 10 in my case) and $T_{d\omega} = 3T_s + \frac{T_{s\omega}}{2}$ is the dead time of the speed control loop. The calculated parameters are

$$K_{\omega} = 0.5191 \quad \text{and} \quad T_{\omega} = 8.000 \times 10^{-3} \text{ sec.}$$

It is important to mention that using the loop with these control parameters shows great performance when the speed and the position of the rotor are known, but in case of using the outputs of the estimators the dynamics of the system is changed significantly. Delays of the system are drastically increasing when the estimated ω and θ values are fed back to the speed controller, hence quite large oscillations can be seen in the angular velocity of the rotor. For acceptable performance in sensorless operation, retune of the speed controller is required.

Figure 5.1 demonstrates the operation of the control loop. It can be seen that the step response of the angular velocity follows the reference signal with minimal overshoot while the steady state is smooth and oscillation free.

5.2 High frequency alternating signal injection

In the simulations it was assumed that the initial position of the rotor is known, hence the first presented method is the high frequency alternating signal injection. The method's theory was introduced in 4.2. During the operation a low voltage AC signal is injected into either the q or the d axis voltage, the parameters of this signal needs to be set appropriately. Both the amplitude and the frequency of the injected sine wave was chosen as the tenth of the nominal DC voltage and the

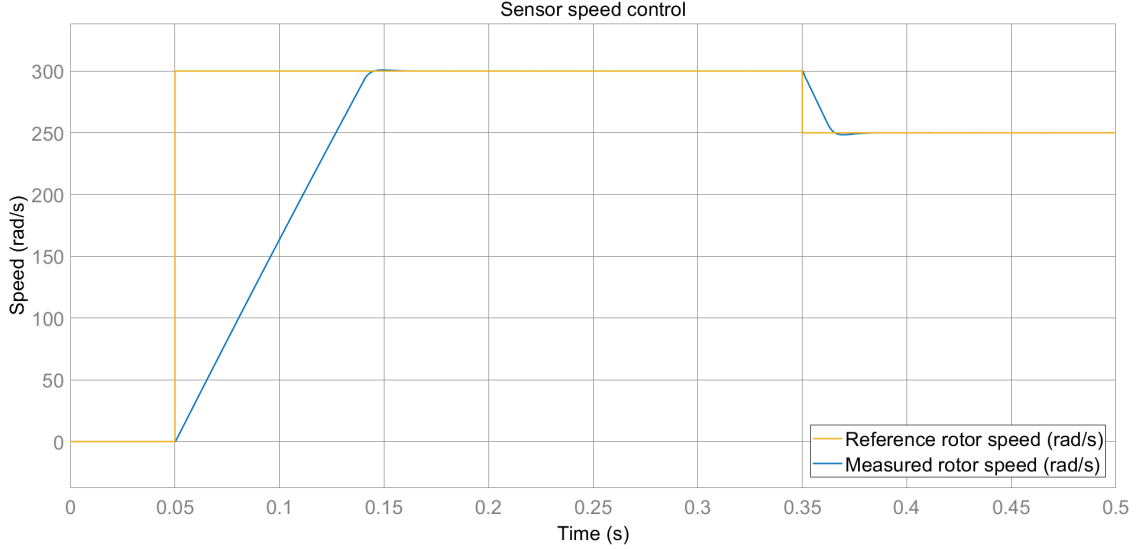


Figure 5.1: Operation of the speed control loop using sensors.

inverter switching frequency [12], hence the parameters of the signal are

$$V_{inj} = 2.4 V$$

$$\omega_h = 2\pi \times 1 kHz.$$

The signal must be added to the d axis voltage directly before applying the inverse transformations on the $d-q$ rotating frame signals. As the signal was injected into the d axis, the estimation process needs to use the q axis current as an input.

5.2.1 Structure of the simulation model

Firstly, the estimator processes the input q -axis current by using multiple filters and creates a signal that is proportional to the error of the rotor position value as described in eq. 4.9. First a band-pass filter should be applied to the input current signal that only let through the high frequency component of i_q . This is achieved by using a series of high-pass and low-pass filters with a cut-off frequency of 1 kHz, thus only the injected component of the AC signal remains. An orthogonal signal component needs to be multiplied into the filtered signal, which needs to be delayed a bit, as the filtering results delay on the input current. One more low-pass filter is applied on the signal, that produces the output, which is a signal proportional to the error of θ_e .

Secondly, a PI tracking loop produces the estimated position and speed in such a way that the error of θ_e tends to zero. In order to make this loop work properly, the estimated values must be fed back to the FOC control loop. As the input signal is

proportional to the error of θ_e , in case of a correctly estimated position the input of the controller will be zero. The values of the gains were chosen via parameter sweep, which was done by using MATLAB's *parsim* function. This allows us to sweep multiple parameters simultaneously and to run several simulations on more CPUs parallelly. The controller gains after multiple simulations were chosen as $P = 250$ and $I = 100000$.

The injected signal is contained by the current feedback lines which results that the raw signals are quite noisy for the current controllers. To get rid of the additional component a low-pass filter could be applied on the q and d axis current too. During the simulations it was found out that the filtering process adds too much delay to the system, hence a more dynamic current and speed control could be achieved without filtering, even with the noisy feedback signals. It is important to understand that filtering the signals is always a trade-off between system dynamics and noisiness. If filters are applied to the current signals, then the high-frequency noise will be reduced and all the other signals will be smoother, but this case a slower current controller is also required to handle the greater dead time. Furthermore, a slower current control loop results a slower speed control loop as well. In this section both solutions will be presented, but later, when the two estimators will be combined, the non-filtered version will be chosen. If a more precise control is required at lower speeds, it is worth considering to use a filtered current feedback line and slower controllers, but in my case this estimator is used mostly in transient states, therefore, dynamics are preferred over less noisy signals.

The numerous filters applied in this process changes the dynamics of the system drastically. So much delay is added to the system that the original controllers are not able to work properly anymore. The speed controller of the FOC must be retuned in order to make the high frequency alternating signal injection method work. The transfer function of the current controller is the same as in eq. 5.3 and the new gains were chosen as

$$K_{\omega,inj} = 0.1093 \quad \text{and} \quad T_{\omega,inj} = 0.0380 \text{ sec.}$$

5.2.2 Results of the simulation

With these controller parameters the estimator was robust enough to extract the position and speed information, that can be seen on figure 5.2 and 5.3. It can be seen that the cosine of θ is really close to the measured value, only a slight difference is visible immediately after starting. The estimated speed signal is pretty noisy as

filters were not used, even so the controller is able to follow the reference speed throughout the whole process.

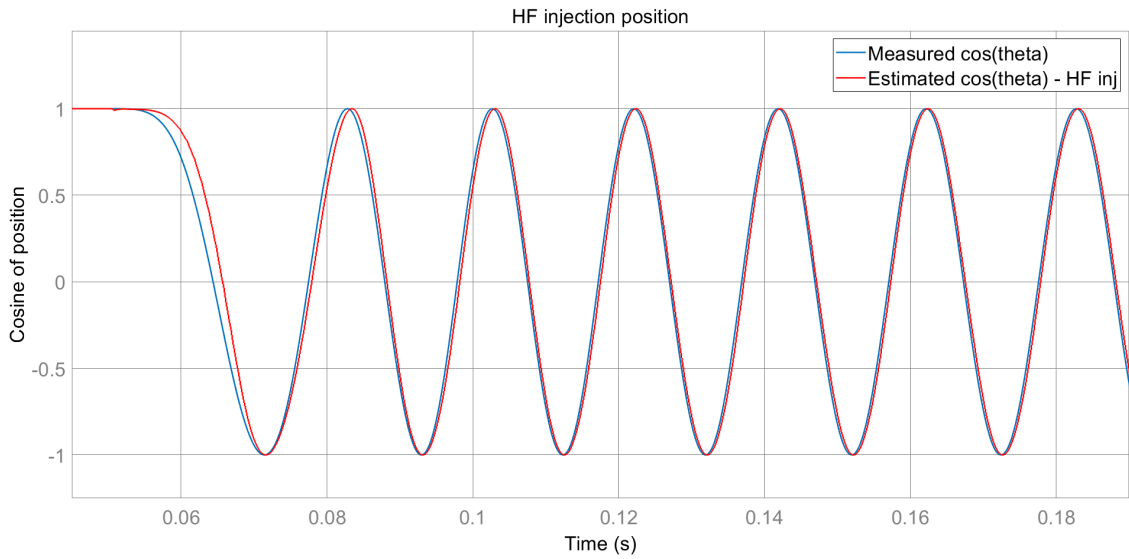


Figure 5.2: Position estimation with the high frequency injection method.

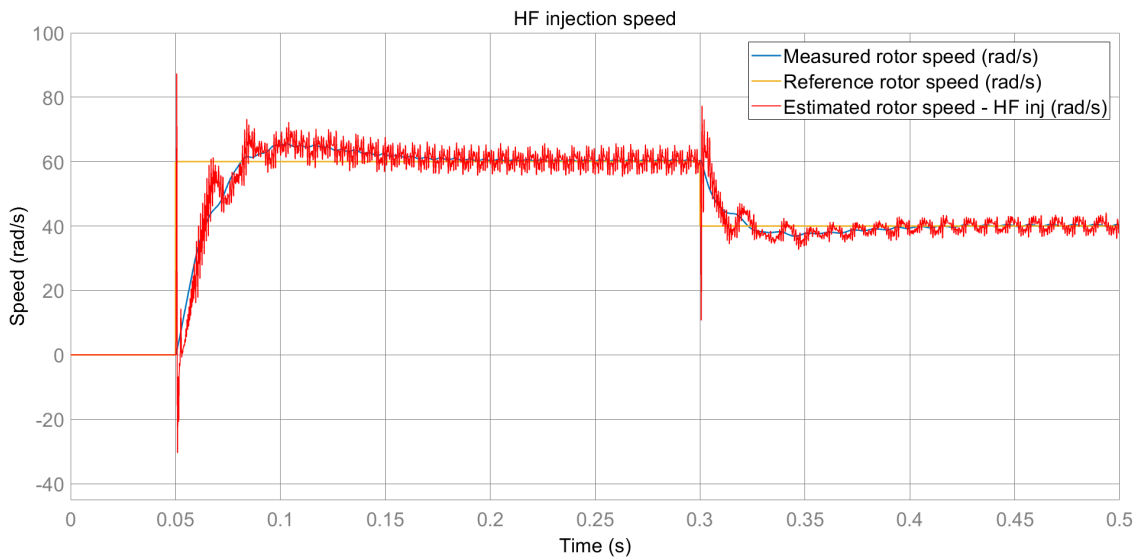


Figure 5.3: Speed estimation with the high frequency injection method.

On figure 5.4 the biggest drawback of signal injection methods is presented. As a high frequency signal is added to the d -axis voltage, the HF component will be transformed back to the abc frame as well, hence the phase currents will be distorted. Even though the sinusoidal form somewhat visible, some kind of beat effect (like in acoustics) can be seen.

The estimator is highly dependent on the L_d and L_q inductances, as the method can be used only if they are not equal. On figure 5.5 a parameter sensitivity test can be seen, where the inductances were changed during the simulation. At $t =$

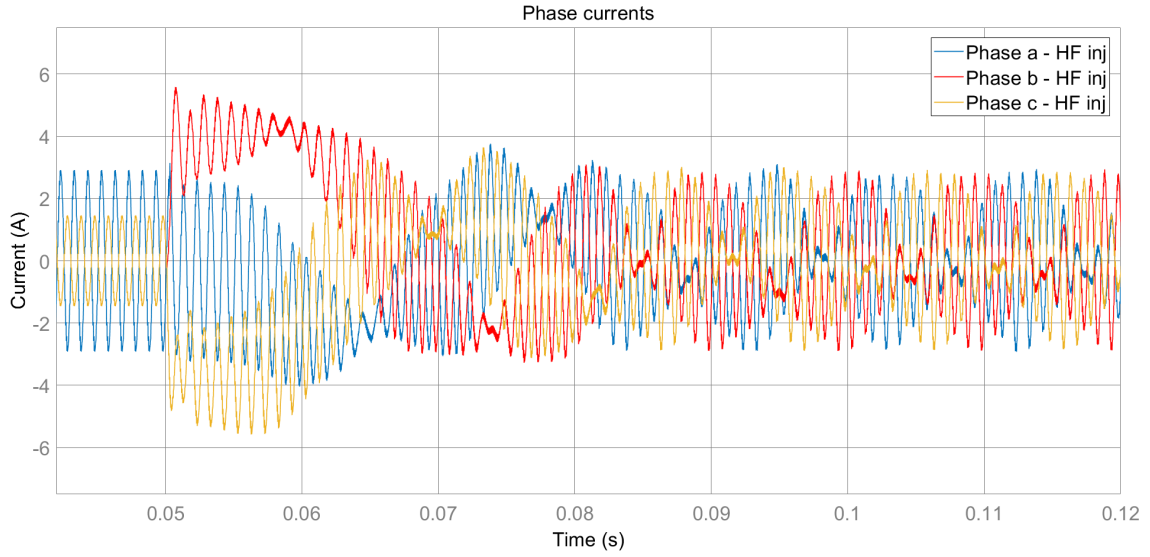


Figure 5.4: Phase currents with signal injection.

0.3 s the value of L_d was increased by 20% and at $t = 0.45$ s L_q was decreased by also 20%. It can be seen that the first change did not effect the speed control too much, but after the second one significant oscillations start to appear. Even though the estimated speed got more noisy, the process was robust enough to keep up the control. It must be mentioned that the estimator is based on the high frequency inductances and the simulation does not consist of these kinds of effects like saturation, hence at real motors the estimation can be even more robust for closer L_d and L_q values.

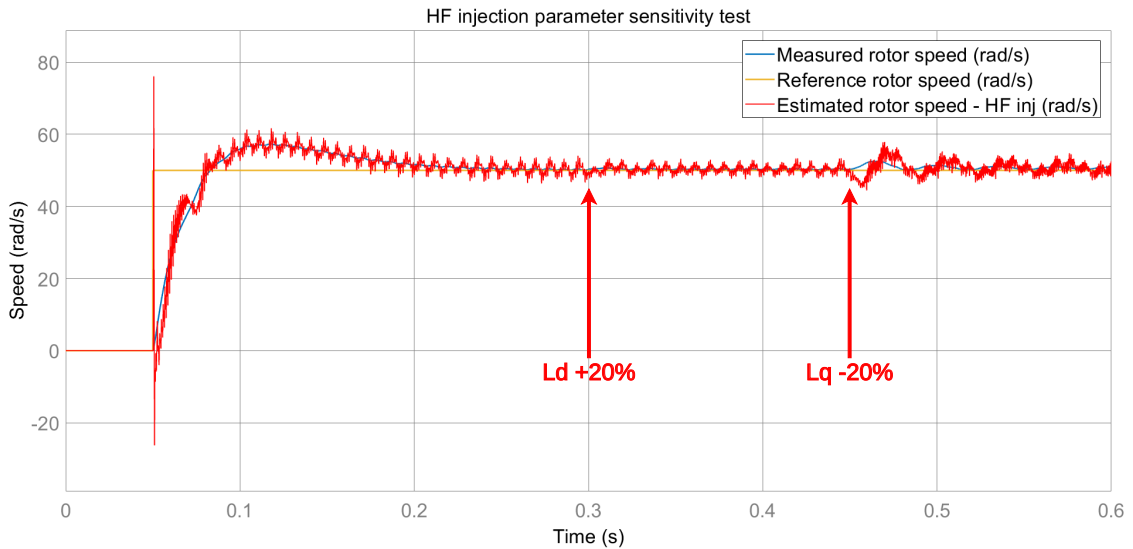


Figure 5.5: Parameter sensitivity test by changing L_d and L_q during the control process.

As previously mentioned, the noise of the estimator can be reduced by filtering the current feedback lines. For both i_d and i_q a first-order low-pass filter was used to get rid of the high frequency component. At i_d the cut-off frequency was set to $\frac{\omega_h}{10}$, because most of the high frequency component can be found in this signal as the additional component was injected into the d -axis. On the other hand at i_q the high-frequency component is less significant, hence the cut-off frequency was set to $\frac{\omega_h}{5}$ only, to improve the dynamics slightly.

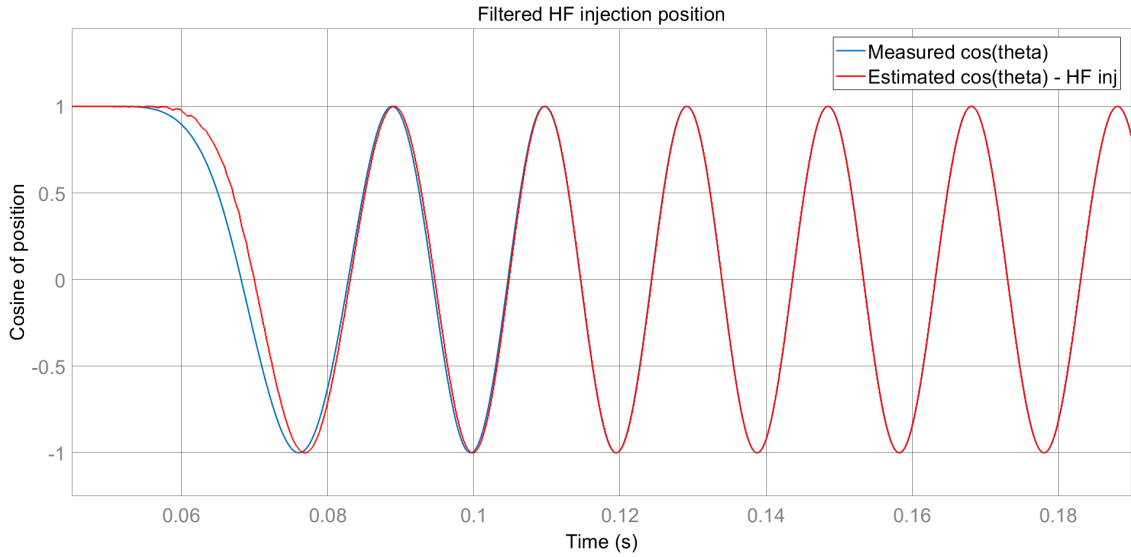


Figure 5.6: Position estimation with the high frequency injection method, when currents are filtered.

The current controllers and the speed controller had to be retuned once again to compensate the additional delay of the filters. The new controller parameters are

$$\begin{aligned}
 K_{id,inj_filter} &= 0.2333 & \text{and} & & T_{id,inj_filter} &= 1.0368 \times 10^{-3} \text{ sec} \\
 K_{iq,inj_filter} &= 0.4778 & \text{and} & & T_{iq,inj_filter} &= 1.8088 \times 10^{-3} \text{ sec} \\
 K_{\omega,inj_filter} &= 0.0865 & \text{and} & & T_{\omega,inj_filter} &= 0.0480 \text{ sec.}
 \end{aligned}$$

On figure 5.6 and 5.7 the estimated position and speed is presented with using the aforementioned current filters and returned controllers. It can be clearly seen that both the position and the speed values are closer to the measured results and the noise had been reduced visibly. In contrast, the step response is slower compared to figure 5.3, where the steady state was reached around 0.05 seconds faster.

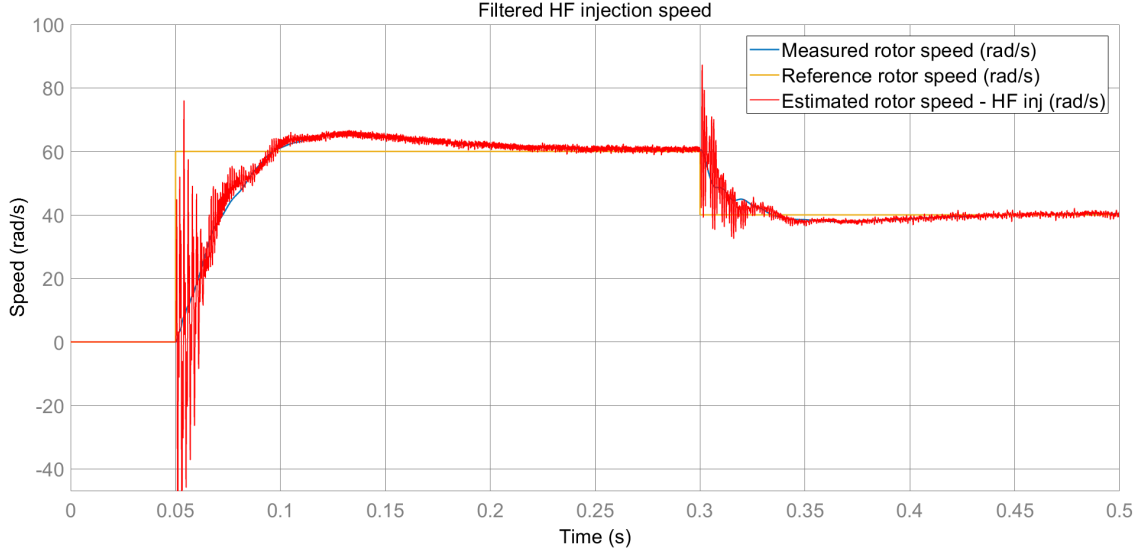


Figure 5.7: Speed estimation with the high frequency injection method, when currents are filtered.

5.3 Luenberger observer

The theory of the Luenberger observer was introduced in 4.3. The observer gains were designed both for the simplified model, where the L_d and L_q inductances are similar, and for the more complex model (called advanced Luenberger observer from now on), where the A matrix is dependent on the estimated speed. Both of the observers used the discretized model, as the control loop runs in discrete time.

5.3.1 Observer design

The equation that needs to be solved each case is the following

$$\det(z\mathbf{I} - (\mathbf{A}_{DI} - \mathbf{L}_{DI}\mathbf{C}_{DI})) = (z - p_{DI})^4 \quad (5.5)$$

where the matrices are the same as in section 4.3, $p_{DI} = e^{-pT_s}$, where the time constant of the observer is $-\frac{1}{p}$ and L is the observer gain that can be written as

$$\mathbf{L}_{DI} = \begin{bmatrix} g_{i\alpha} & 0 \\ 0 & g_{i\beta} \\ g_{e\alpha} & 0 \\ 0 & g_{e\beta} \end{bmatrix}. \quad (5.6)$$

In order to achieve great performance and get a fast enough observer the value of p has to be chosen carefully. A too small p results a too slow observer which

is not able to follow the system, while a too large p can cause oscillations at the output of the observer. It is a good practise to choose p one order of magnitude faster than the electrical time constant of the machine. In the simulation the fastest electrical time constant is the one that corresponds to the d axis and its value is $T_{ad} = \frac{L_d}{R_s} \approx 7.3684 \times 10^{-4} \text{ sec}$. To this constant at least a value of $p \approx -13500$ is required, hence a bit faster pole was chosen $p = -15000$, which means the discrete pole needs to be around $p_{DI} = 0.2231$.

After solving the equation the calculated gains of the simplified observer is the following.

$$g_{i\alpha} = g_{i\beta} = 1.4647 \quad \text{and} \quad g_{e\alpha} = g_{e\beta} = -1.9313 \quad (5.7)$$

For the advanced observer model the design was a bit more complicated because the equation had to be solved for different speeds. As the gains do not change too much for greater change in the speed, I chose a step size of $\Delta\omega = 30 \text{ rad/s}$, so an observer design was needed for every 30th value. The first equation was written for $\omega = 15 \text{ rad/s}$ and the result was used in the $0 - 30 \text{ rad/s}$ speed range. The second equation was written for $\omega = 45 \text{ rad/s}$ and corresponded to the $30 - 60 \text{ rad/s}$ range, etc. The maximum design speed was $\omega = 375 \text{ rad/s}$, because it is already over the machine's top speed. Unfortunately as a reason of the more complex matrices, eq. 5.5 had 6 solutions for every ω value, which made the design even more complicated. Most of the results were complex numbers, thus logically one of the real solutions needed to be chosen.

After the design process was completed for all speed values, I got the results that are presented in table 5.1, where the first value corresponds to $\omega = 15 \text{ rad/s}$, while the last value is for $\omega = 375 \text{ rad/s}$. It can be seen even though the gains are close to each other for different speeds, at higher angular velocity the difference between α and β -axis values starts to increase.

Observer gains					
Gain	$\omega = 15 \text{ rad/s}$	$\omega = 45 \text{ rad/s}$...	$\omega = 345 \text{ rad/s}$	$\omega = 375 \text{ rad/s}$
$g_{i\alpha}$	1.4180	1.4181	...	1.4197	1.4198
$g_{i\beta}$	1.4180	1.4180	...	1.4164	1.4162
$g_{e\alpha}$	-1.2674	-1.2625	...	-1.1420	-1.1420
$g_{e\beta}$	-1.2674	-1.2723	...	-1.3774	-1.3867

Table 5.1: The gains of L_{DI} for different ω values.

5.3.2 Structure of the simulation model

The whole estimation process can be split into two main steps, firstly determine the back EMF values via the observer and secondly get the estimated position and speed by using only the back EMF. The input currents and voltages are given in the α - β stationary frame, and connected directly to the observer. The structure and the gains of the Luenberger observer block are the same that were presented on the block diagram on figure 4.3. For the more complex model instead of constant \mathbf{A}_{DI} , \mathbf{B}_{DI} , \mathbf{C}_{DI} and \mathbf{L}_{DI} matrices, a look-up table was used to choose the proper matrix. At the output of the delay block the estimated internal states of the system can be found which consists the back EMF values (e_α and e_β) as the third and fourth component.

As the back EMF values are produced, we can calculate $\sin(\hat{\theta})$ and $\cos(\hat{\theta})$ as in eq. 5.8 [22]. The final step is to get the estimated ω and θ which can be done by using a PI tracking loop, similar to the one that was introduced at the end of the high frequency alternating signal injection process. The input error signal of the PI loop was given in chapter 4 with eq. 4.3.4.

$$\sin(\hat{\theta}) = -\frac{\hat{e}_\alpha}{\sqrt{\hat{e}_\alpha^2 + \hat{e}_\beta^2}}, \quad \cos(\hat{\theta}) = \frac{\hat{e}_\beta}{\sqrt{\hat{e}_\alpha^2 + \hat{e}_\beta^2}} \quad (5.8)$$

In the tracking loop besides the PI gains, signal filtering also takes place. A first-order low-pass filter was used in order to remove the high frequency noise that is produced by the P component of the tracking loop. The filtering process makes the ω_e output signal a bit smoother but also brings some more delay into the system. The chosen gains of the tracker are $P = 100$ and $I = 150000$ in case of the advanced observer, and $P = 250$ and $I = 50000$ for the simplified observer. These values were determined by MATLAB/Simulink parameter sweep and showed acceptable performance during the tests.

5.3.3 Results of the simulation

Even though the Luenberger observer could work with the faster speed controller, during the tests it used the same controller as the signal injection method, because, when the estimators are combined then the slower controller must be used anyway.

5.3.3.1 Open-loop operation

Graph 5.8 and 5.9 demonstrates the functioning of the speed estimator in open-loop operation. It can be seen that at low speeds (under 50 rad/s) the estimated ω is noisy and inaccurate, hence as the theory also stated this estimator can be used only at higher speeds. The graph also shows that over 50 rad/s the estimator works correctly and follows the actual rotor speed value with minimal difference.

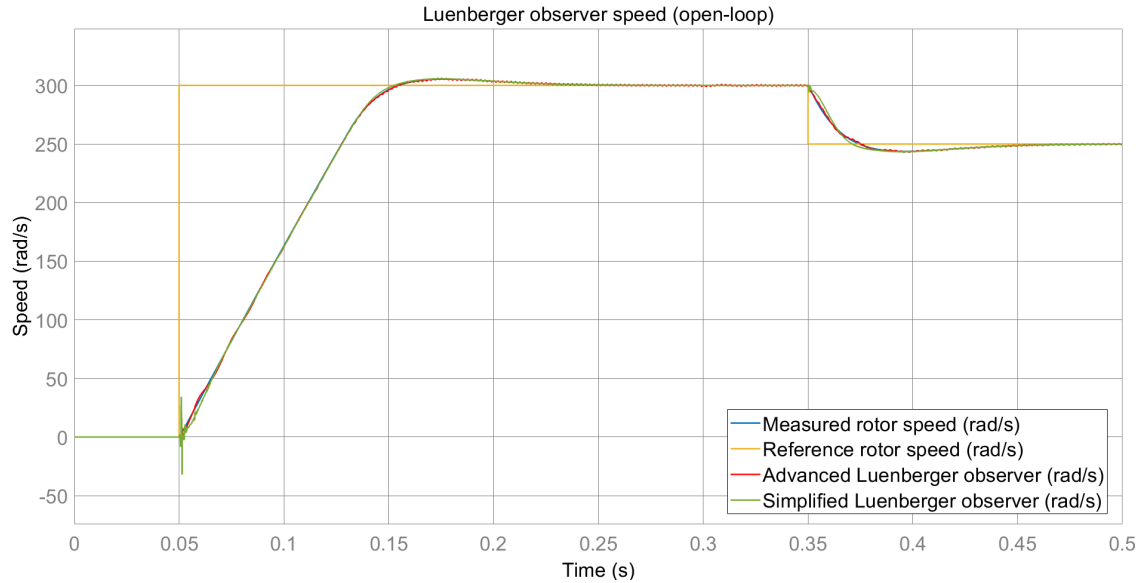


Figure 5.8: Speed estimation of the two Luenberger observers in open-loop operation.

On 5.9a it can be seen that the simplified Luenberger observer reacts slower and it is less accurate at lower speeds. Graph 5.9b and 5.9d demonstrated that at transient states the advanced observer shows faster response and better performance as it is closer to the measured speed. In contrast, at steady state (figure 5.9c) the advanced estimator has a constant oscillation with an amplitude of 0.5 rad/s , while the simplified model results an almost constant value.

5.3.3.2 Advanced Luenberger observer

When the control performance of the observers were tested, at startup the sensor control was used and the control process switched to the observer over 100 rad/s , as the observer can not be used at lower speeds. Firstly the advanced Luenberger observer will be demonstrated, followed by the simplified one.

Figure 5.11 and 5.12 show the position and speed estimation of the advanced observer during control. It can be seen that the estimated position has a small offset compared to the measured one, but it has no effect on the control process. At the speed diagram

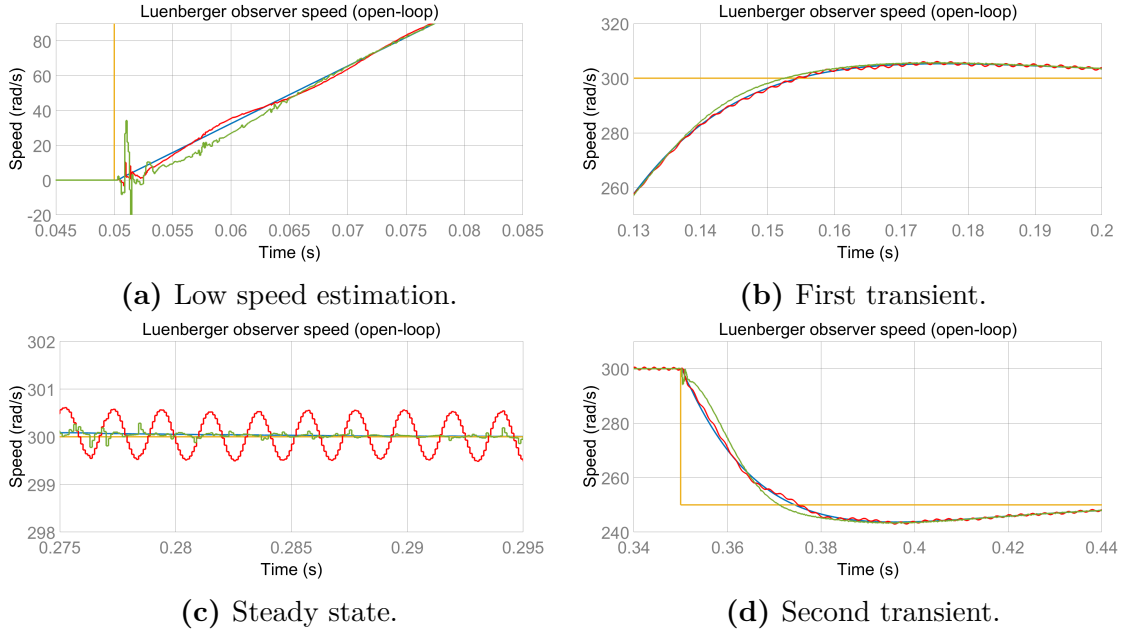


Figure 5.9: Detailed diagrams of the operation of the speed estimator.

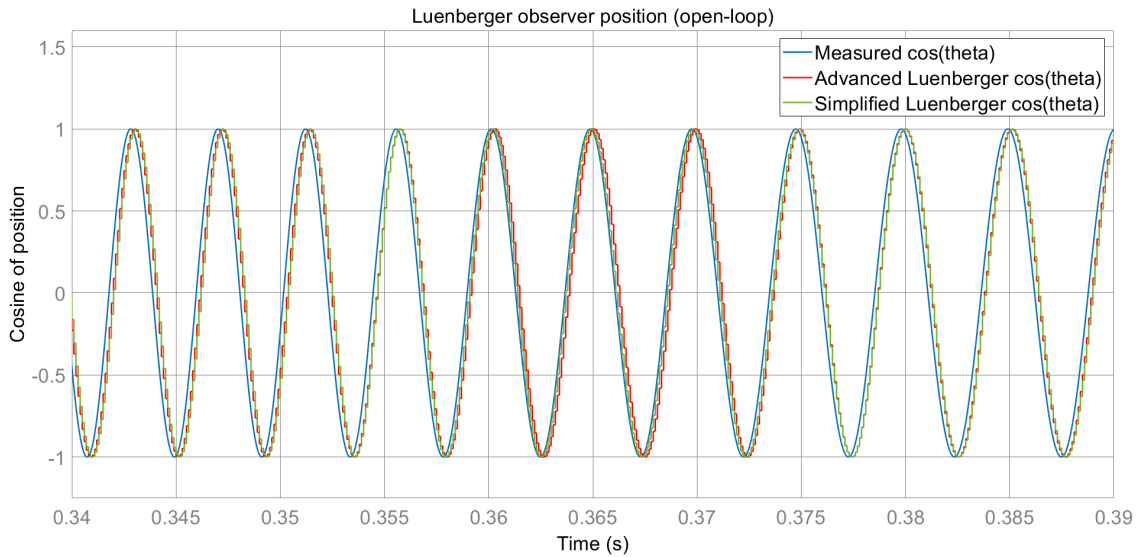


Figure 5.10: Position estimation of the two Luenberger observers in open-loop operation.

the oscillation at steady state appears again and has a minor effect on the speed control at 300 rad/s .

On 5.13 the stator currents are presented, which have the expected sinusoidal form. If we compare this to figure 5.4, we can see the biggest advantage of using the Luenberger observer. While at the signal injection method the estimation process effected directly to the machine as the stator currents were highly distorted, here the observer has just indirect effects on the system. On 5.13 the wave forms also show the oscillations at steady state.

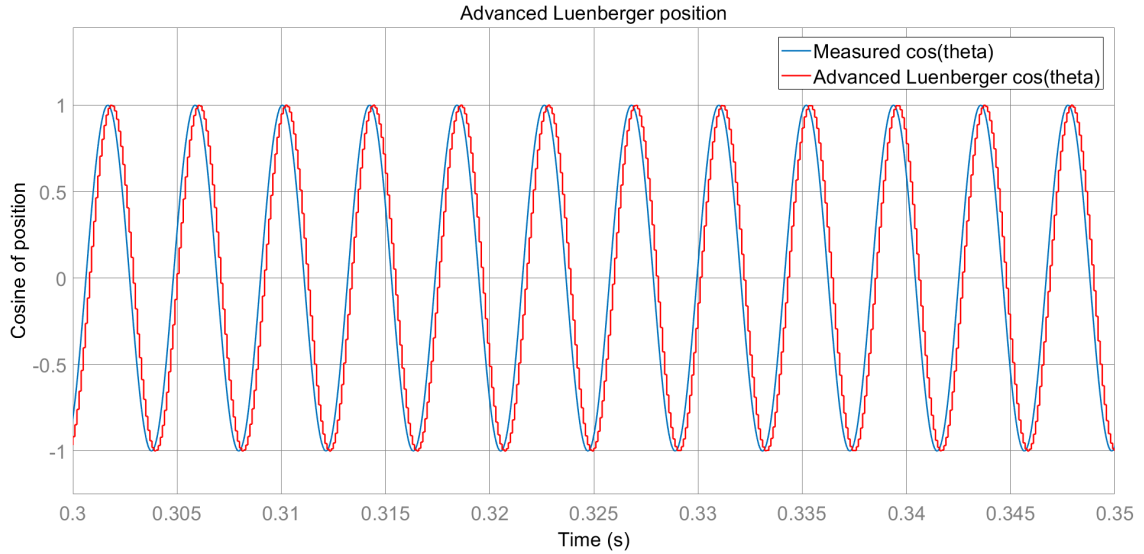


Figure 5.11: Position estimation of the advanced Luenberger observer in closed-loop operation.

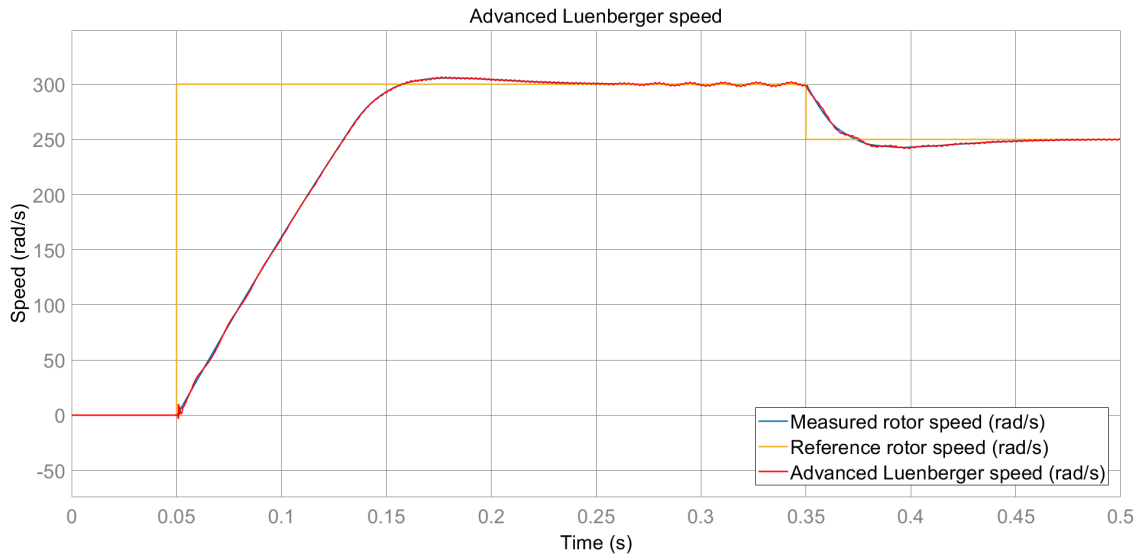


Figure 5.12: Speed estimation of the advanced Luenberger observer in closed-loop operation.

5.3.3.3 Simplified Luenberger observer

Figure 5.14 and 5.15 present the performance of the simplified Luenberger observer. At steady state the position estimation is really similar compared to the advanced observer, but the estimated speed has no oscillation.

As expected, during transient state the simplified observer follows the speed less accurately, but it has no effect on the control performance. During the acceleration phase a small peak can be noticed, when the control loop switches from sensor to sensorless operation, but this has no consequence for the control process either.

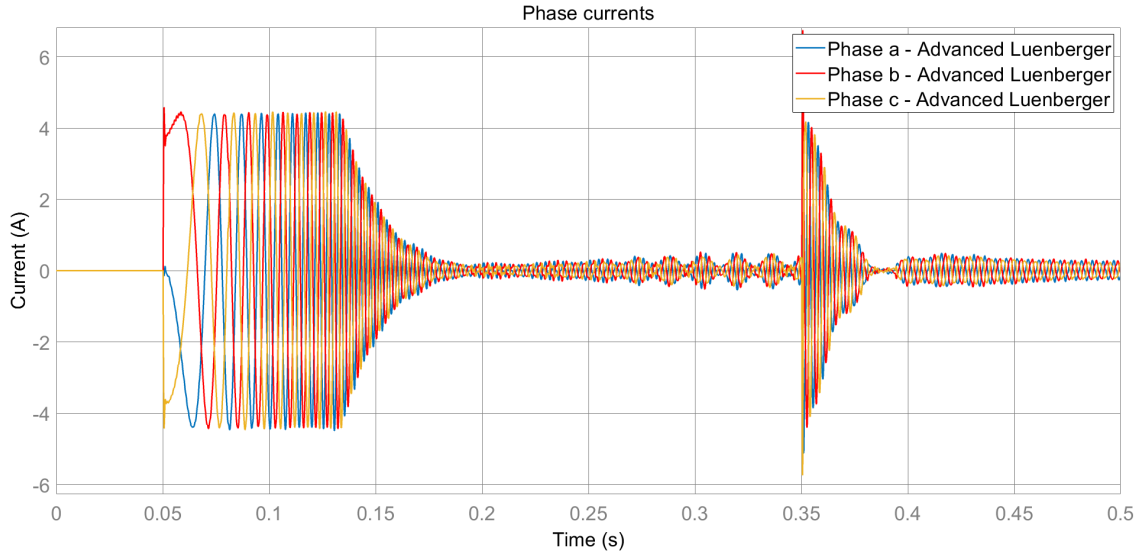


Figure 5.13: Phase currents when the advanced Luenberger observer is used.

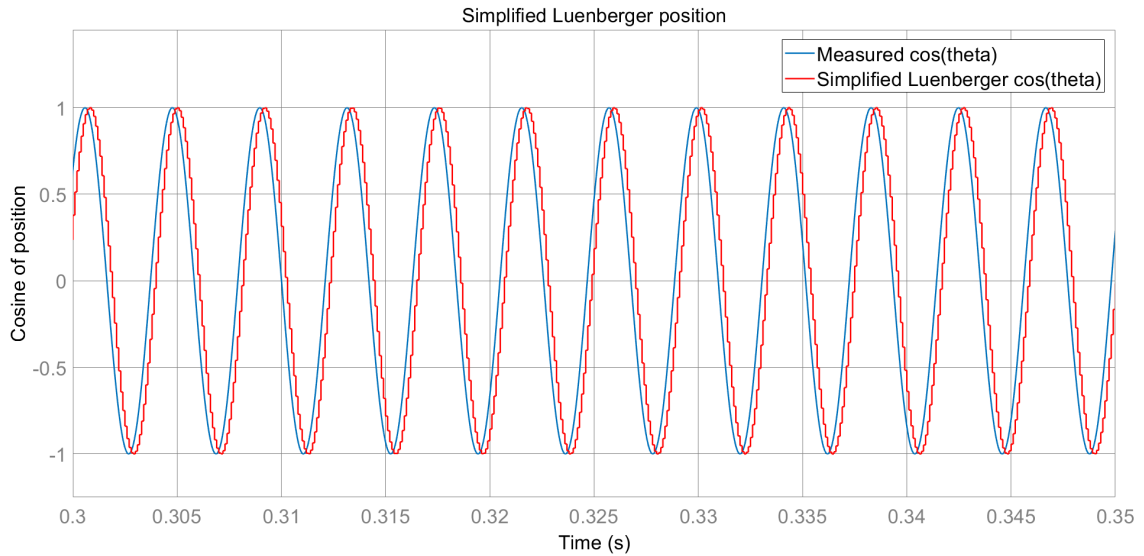


Figure 5.14: Position estimation of the simplified Luenberger observer in closed-loop operation.

This effect was not visible at the advanced observer as it handled the transients more effectively.

The stator currents in this case are also very similar to the advanced observer's wave forms. The main difference can be noticed at steady state, where the oscillations do not appear this time, hence the signal shapes look slightly better.

5.3.3.4 Parameter sensitivity tests

In order to demonstrate and compare the robustness of the previously presented Luenberger observers, parameter sensitivity tests were made. Both cases the value

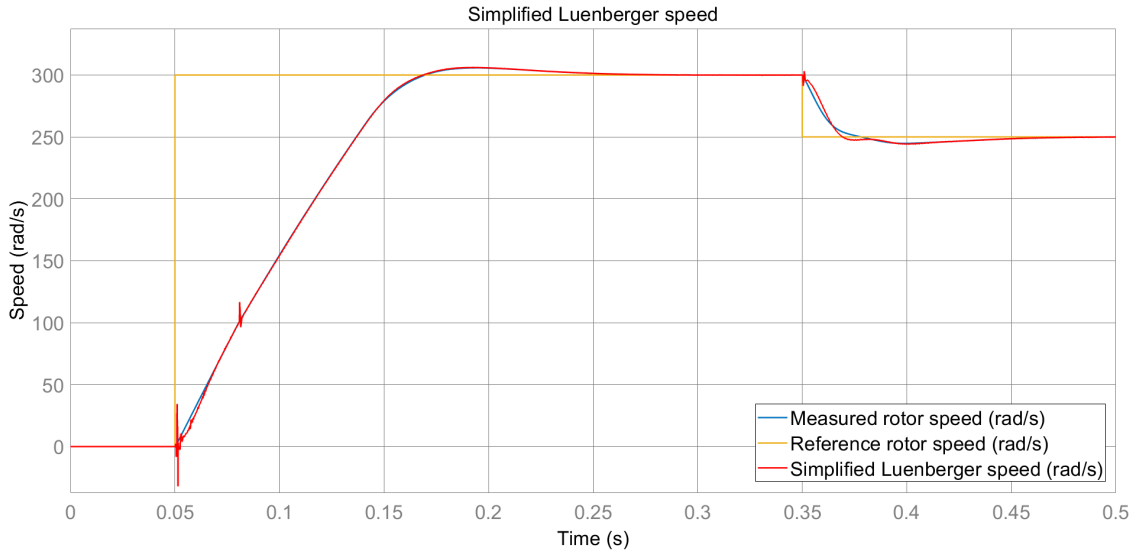


Figure 5.15: Speed estimation of the simplified Luenberger observer in closed-loop operation.

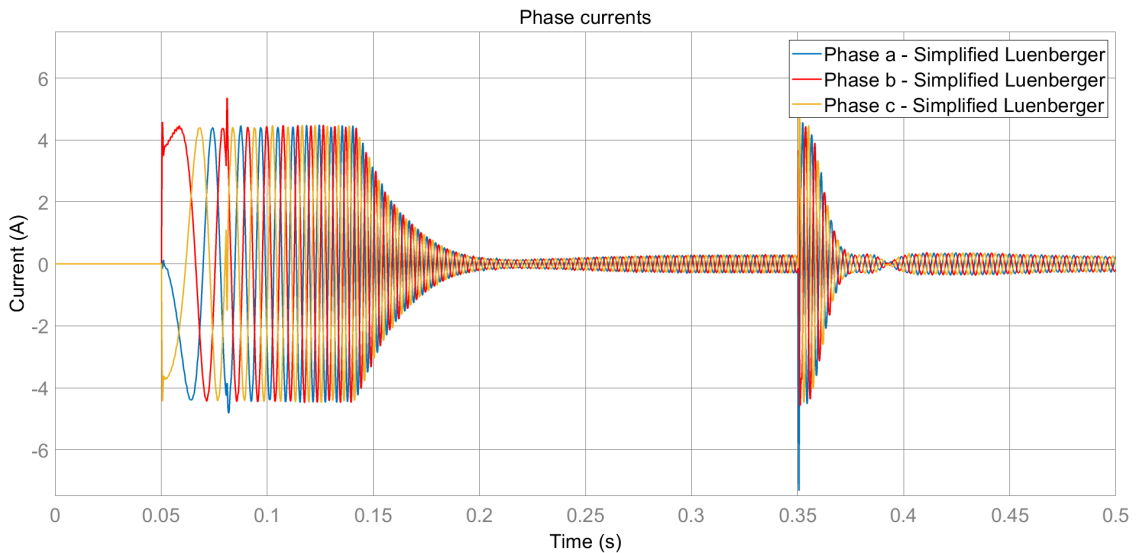


Figure 5.16: Stator currents when the simplified Luenberger observer is used.

of L_d and L_q inductances were changed during the simulation by 40%. The first change occurred at $t = 0.3 \text{ sec}$ when L_d was modified, then L_q was switched at $t = 0.45 \text{ sec}$.

In the advanced model we took advantage of the difference in inductance values, hence it effects more to the observer, when L_d and L_q get closer to each other. Figure 5.17 and 5.18 show the effect of parameter changes, it can be seen that while the first value change has only minor effect, the second one (figure 5.18b) results noticeable oscillation.

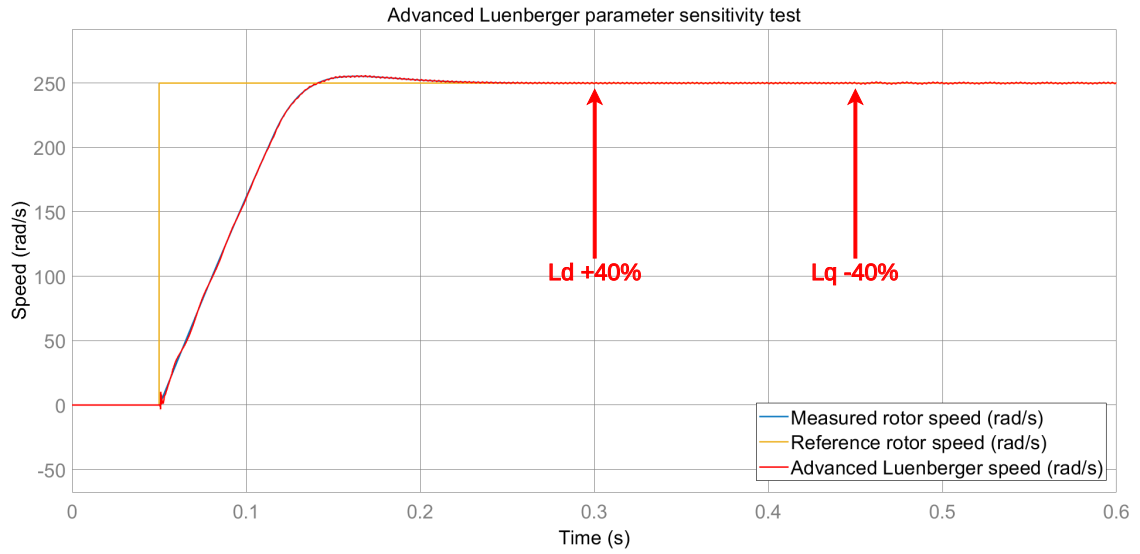


Figure 5.17: Parameter sensitivity test by changing L_d and L_q during simulation.

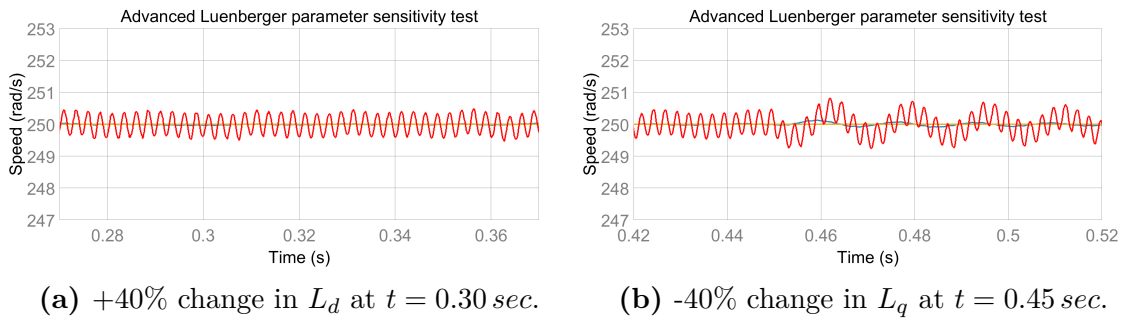


Figure 5.18: Detailed diagrams of the effect of parameter change.

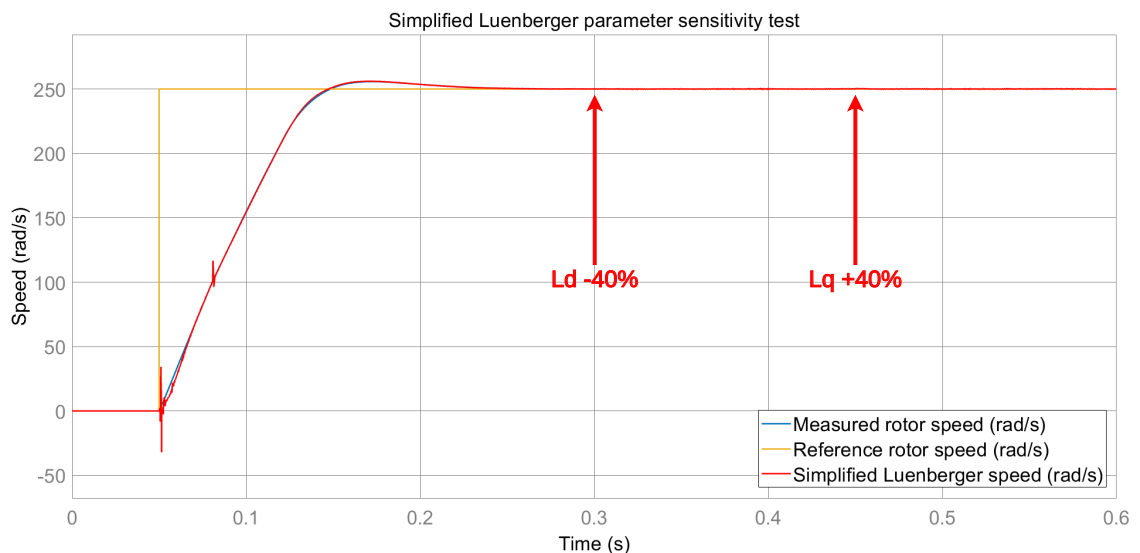


Figure 5.19: Parameter sensitivity test of the simplified Luenberger observer.

Almost the same test was completed for the simplified model, but now the direction of the inductance change is reversed, its results are shown on figure 5.19 and 5.20.

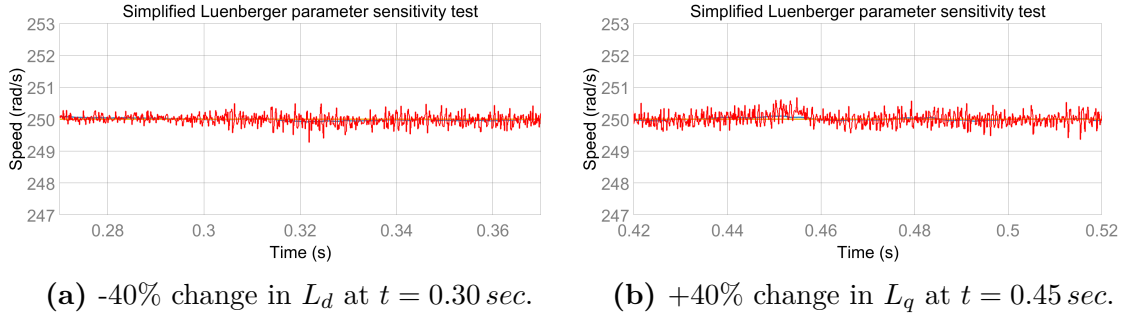


Figure 5.20: Detailed diagrams of the effect of parameter change.

As this model calculates with equal L_d and L_q the even bigger gap between them effects the observer more. It can be seen on figure 5.20a and 5.20b that the value changes cause a bit more noise, but the effect is negligible. It can be say that the simplified Luenberger observer is more robust and tolerates disturbances better.

5.4 Combining the estimators

As it was previously mentioned, two estimators need to be used in order to control the system the whole operational speed range. The most difficult part of combining these methods is the switching logic that allows us to switch between the signal injection method and the observer back and forth during operation. In this project a speed range was chosen where the switching process can be done. Under 80 rad/s the high frequency signal injection is used, while over 120 rad/s only the observer determines the speed and position information. Between these limits a linear transition was implemented, based on the estimated rotor speed.

The switching between the methods is handled by a state machine, which has four states: only signal injection, accelerating mixed state, only Luenberger observer and decelerating mixed state. The mixed states have a hysteresis, in order to prevent an immediate switch back to the previous state in case of noisy speed signal.

When the high frequency estimator is not in use, the signal injection is suspended to reduce the unnecessary noise in the system. In case of switching back from the observer to the injection method the high frequency signal needs to be restarted. If it would be resumed at the begin of the mixed state, then the estimator would not have enough time to reduce the position error and get in sync [12], hence the additional signal is started again earlier, at 160 rad/s .

On figure 5.21 a simulation is shown, where the combined estimators were used and the switching process is presented both directions. The first transition can be noticed around $t = 0.09 \text{ sec}$, while the back switch happens around $t = 0.53 \text{ sec}$.

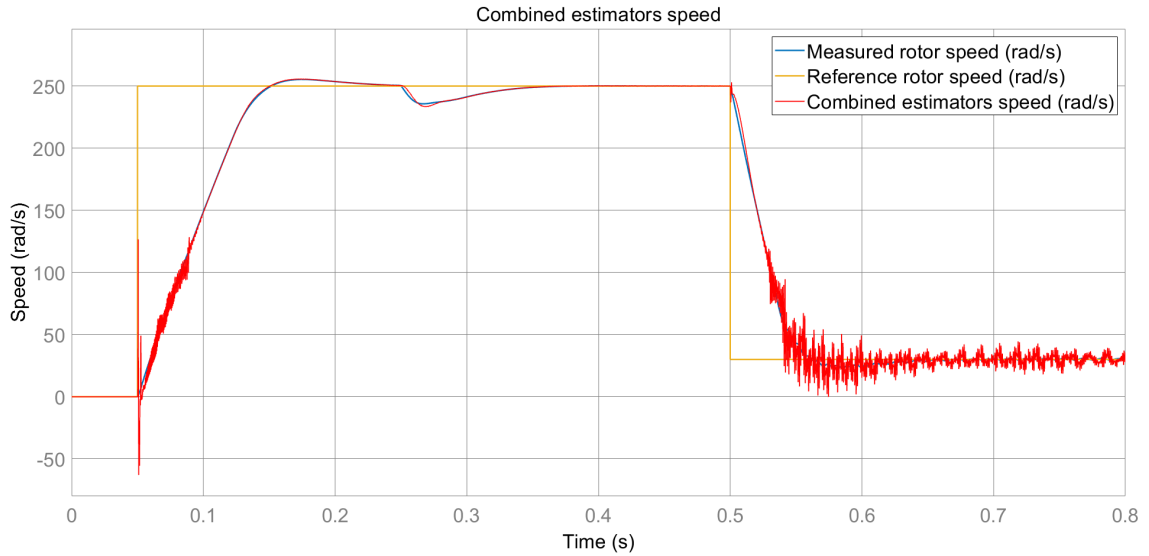


Figure 5.21: Estimated speed profile with additional torque load.

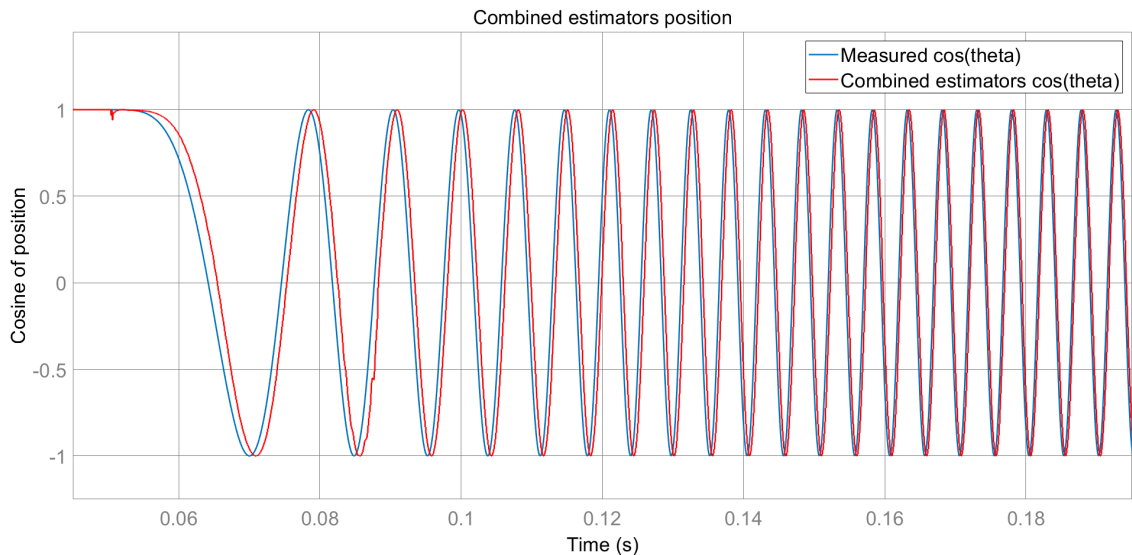


Figure 5.22: Position determined by the two estimator methods.

At $t = 0.25 \text{ sec}$ a 0.12 Nm load torque is added to the machine to demonstrate the disturbance tolerance of the sensorless speed control. It can be seen that the high frequency estimator is really noisy, especially when the additional signal is resumed during the switch back state, however the control is still robust enough. At higher speeds the estimation works much better, the Luenberger observer provides a smooth signal and compensates the additional load perfectly.

Figure 5.22 demonstrates the estimated rotor position from standstill, until only the observer is in use. Around $t = 0.085 \text{ sec}$ a short period can be seen where the transition was done, but the estimated position remained accurate throughout.

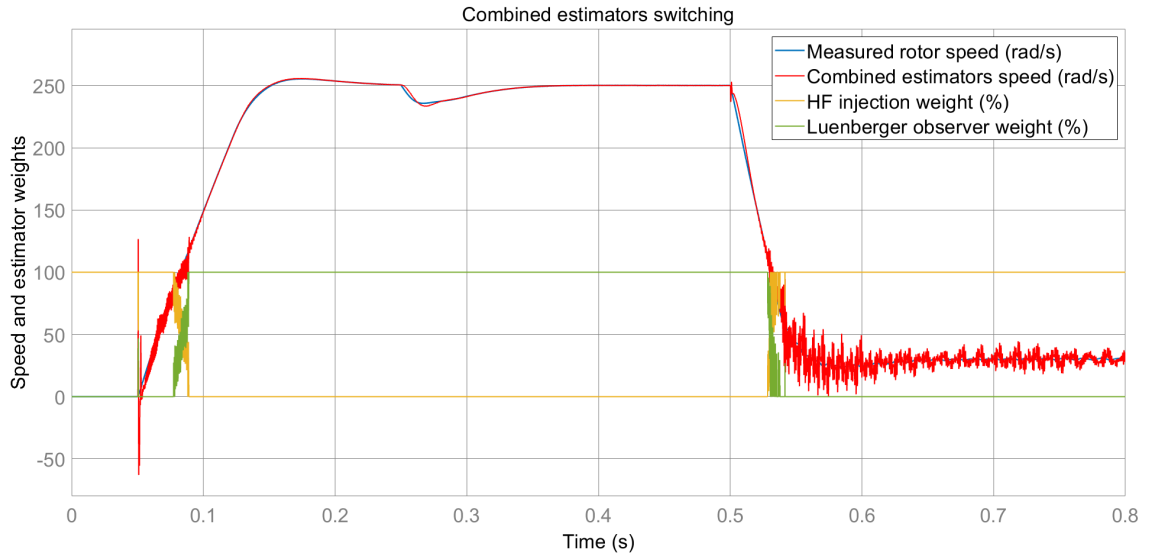


Figure 5.23: Switching between the signal injection and the observer.

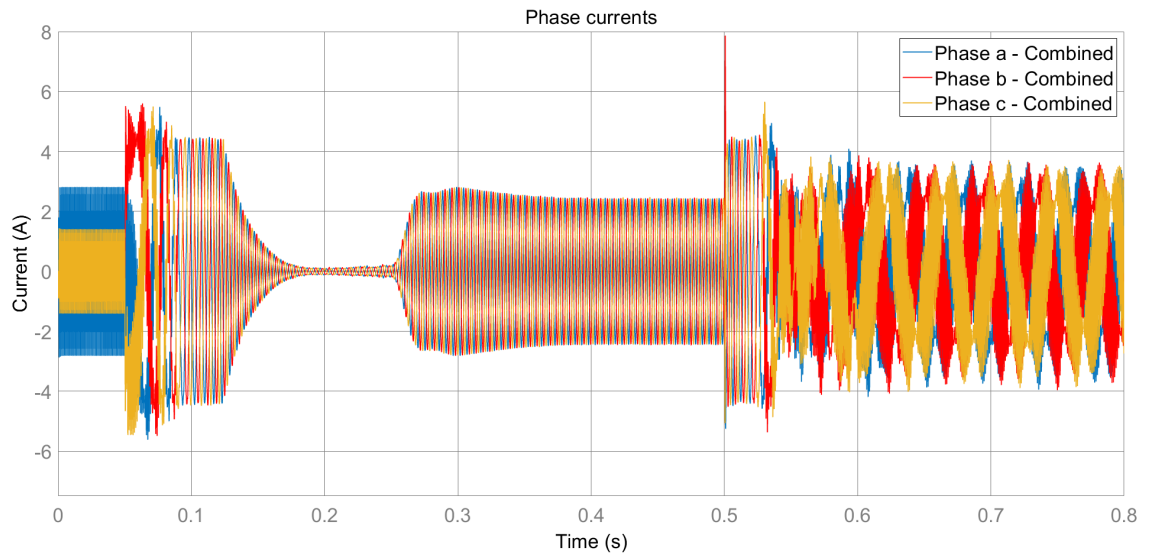


Figure 5.24: Phase currents when the two estimators are used combined.

Figure 5.23 visualizes the linear transition between the estimators. The yellow and green weight signal represent, what percentage is the corresponding estimator contributes to the estimated speed. The linear transition is a bit noisy, because the weights are calculated from the estimated speeds and the weight values from the previous time step.

The phase currents are presented on figure 5.24, where the difference between the signal injection and the observer is visualized perfectly. When the high frequency component is added to the system the currents are distorted, while during the high speed period the sinusoidal forms are look better. It can be noticed that after the

torque load was added at $t = 0.25 \text{ sec}$, higher currents are required to maintain the desired speed.

Chapter 6

Implementation

In this chapter only a short preview is shown about later works, which are related to the implementation of the sensorless methods. The experimental environment is shown on figure 6.1, where a Texas Instruments TMS320F283789D DSP is used to run the implemented code. The attached BOOSTXL-3PhGaNI_n VSI is a 48 V, 10 A three-phase inverter equipped with INA240 current sensors, that is also manufactured by Texas Instruments. The NT Dynamo Brushless DMA0204024B101 SPMSM machine can be seen on the right side of the power supply and it has the following parameters:

- Number of pole pairs: 5
- d and q axis inductances: $L_d = L_q = L_s = 0.32 \text{ mH}$
- Stator resistance: $R_s = 0.285 \Omega$
- Torque constant: $K_t = 0.05917 \frac{\text{Nm}}{\text{A}}$
- Inertia: $J = 7.77 \times 10^{-5} \text{ kg m}^2$
- Viscous damping: $F = 5 \times 10^{-5} \text{ Nms}$

As it was already mentioned, this PMSM is a symmetric machine, where the inductances are equal. The laboratory power supply produced the 24 V input voltage that was connected to the inverter.

The implemented code was generated by MATLAB, as the Simulink model was slightly modified to be suitable for C code generation. Additional hardware specific blocks were added to the model, which could control the analog-to-digital converters, the PWM peripherals and the encoder. The signals of the system could be logged

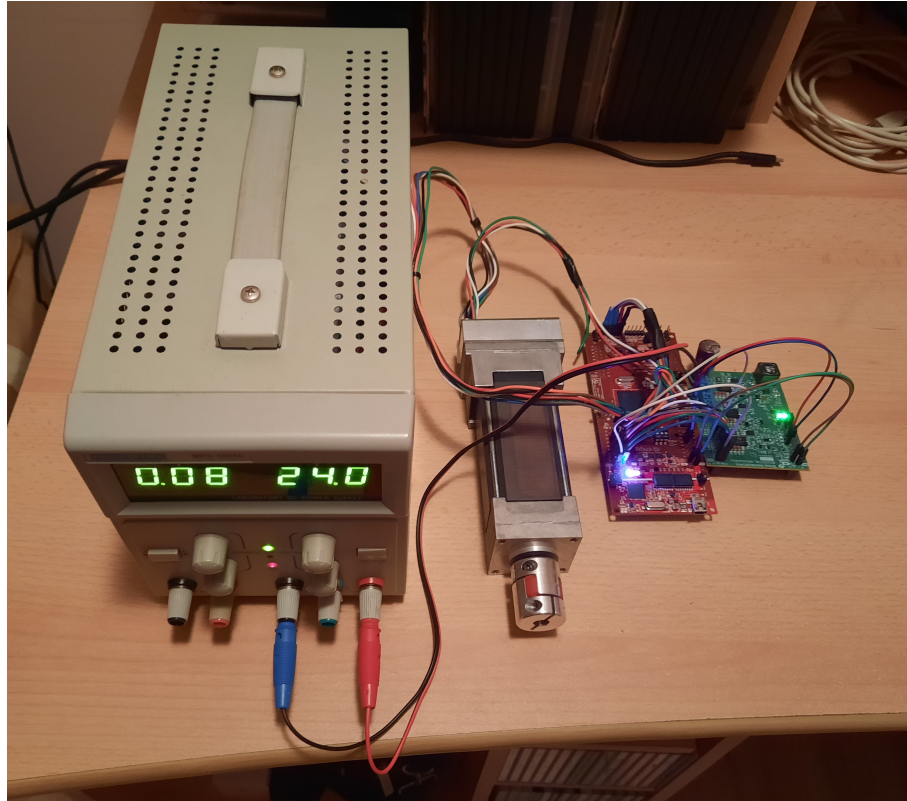


Figure 6.1: Experimental setup including the PMSM machine, the DSP and the 3 phase inverter board.

using the Simulink Monitor & Tune function, which displayed the signals on the Scope attached to the model.

A few rudimentary tests had already been prepared on the physical environment, where the sensor FOC control and the open-loop Luenberger observer were implemented. For the first tries the results were promising as the speed and position estimation worked correctly at higher speeds.

As future work both estimators will be implemented and tested on the real drive. The aim of the project is to demonstrate a robust and reliable fully sensorless PMSM system that allows to control the machine in the entire operable speed range.

Conclusion

This report introduced several existing sensorless methods that can be used to obtain the speed and position of PMSMs. Two of these methods were discussed in detail and then implemented in MATLAB/Simulink.

The results showed that the combination of high frequency signal injection and Luenberger observer is sufficient to control the machine the whole speed range, however at lower speeds and in transient states the estimated signals were noisy and inaccurate sometimes. It was also found that using sensorless methods made the tune of controllers difficult as the required filters caused additional delay in the system. Several retunes of the current and speed controllers solved the issue of larger dead times, but it also meant that the dynamics of the system got worse and response time was increased. In spite of all these, the control process seemed to be robust enough and the machine reached the reference speed always, even when a torque load was added to the simulation.

It can be said that the introduced sensorless methods worked fine in the simulations and after implementation possibly it will be able to control a real machine using them. Future work will examine the extent to which the simulation results can be transferred to reality and what further implications the use of an SPMSM has. An initial rotor position estimator can be implemented as well, that can be used in case of the machine is in an unknown starting position.

Bibliography

- [1] O. Benjak and D. Gerling. Review of position estimation methods for ipmsm drives without a position sensor part i: Nonadaptive methods. In *The XIX International Conference on Electrical Machines - ICEM 2010*, pages 1–6, 2010. DOI: 10.1109/ICELMACH.2010.5607978.
- [2] O. Benjak and D. Gerling. Review of position estimation methods for ipmsm drives without a position sensor part ii: Adaptive methods. pages 1 – 6, 10 2010. DOI: 10.1109/ICELMACH.2010.5607980.
- [3] O. Benjak and D. Gerling. Review of position estimation methods for pmsm drives without a position sensor, part iii: Methods based on saliency and signal injection. In *2010 International Conference on Electrical Machines and Systems*, pages 873–878, 2010.
- [4] Zhiqian Chen, M. Tomita, S. Ichikawa, S. Doki, and S. Okuma. Sensorless control of interior permanent magnet synchronous motor by estimation of an extended electromotive force. In *Conference Record of the 2000 IEEE Industry Applications Conference. Thirty-Fifth IAS Annual Meeting and World Conference on Industrial Applications of Electrical Energy (Cat. No.00CH37129)*, volume 3, pages 1814–1819 vol.3, 2000. DOI: 10.1109/IAS.2000.882126.
- [5] Mihai Comanescu and Todd D. Batzel. Reduced order observers for rotor position estimation of nonsalient pmsm. In *2009 IEEE International Electric Machines and Drives Conference*, pages 1346–1351, 2009. DOI: 10.1109/IEMDC.2009.5075378.
- [6] P.S. Frederiksen, J. Birk, and F. Blaabjerg. Comparison of two, energy optimizing techniques for pm-machines. In *Proceedings of IECON'94 - 20th Annual Conference of IEEE Industrial Electronics*, volume 1, pages 32–37 vol.1, 1994. DOI: 10.1109/IECON.1994.397745.
- [7] Fabio Genduso, Rosario Miceli, Cosimo Rando, and Giuseppe Ricco Galluzzo. Back emf sensorless-control algorithm for high-dynamic performance pmsm.

- IEEE Transactions on Industrial Electronics*, 57(6):2092–2100, 2010. DOI: 10.1109/TIE.2009.2034182.
- [8] Matthias Hofer, Mario Nikowitz, and Manfred Schroedl. Sensorless control of a reluctance synchronous machine in the whole speed range without voltage pulse injections. In *2017 IEEE 3rd International Future Energy Electronics Conference and ECCE Asia (IFEEEC 2017 - ECCE Asia)*, pages 1194–1198, 2017. DOI: 10.1109/IFEEEC.2017.7992211.
- [9] S. Ichikawa, Zhiqian Chen, M. Tomita, S. Doki, and S. Okuma. Sensorless control of an interior permanent magnet synchronous motor on the rotating coordinate using an extended electromotive force. In *IECON'01. 27th Annual Conference of the IEEE Industrial Electronics Society (Cat. No.37243)*, volume 3, pages 1667–1672 vol.3, 2001. DOI: 10.1109/IECON.2001.975538.
- [10] Ji-Hoon Jang, Jung-Ik Ha, M. Ohto, K. Ide, and Seung-Ki Sul. Analysis of permanent-magnet machine for sensorless control based on high-frequency signal injection. *IEEE Transactions on Industry Applications*, 40(6):1595–1604, 2004. DOI: 10.1109/TIA.2004.836222.
- [11] Joohn-Sheok Kim and Seung-Ki Sul. New approach for the low-speed operation of pmsm drives without rotational position sensors. *IEEE Transactions on Power Electronics*, 11(3):512–519, 1996. DOI: 10.1109/63.491646.
- [12] Dávid Kocsis. Implementation and validation of a transient optimized sensorless control algorithm for pmsms. 2019.
- [13] S. Kondo, A. Takahashi, and T. Nishida. Armature current locus based estimation method of rotor position of permanent magnet synchronous motor without mechanical sensor. In *IAS '95. Conference Record of the 1995 IEEE Industry Applications Conference Thirtieth IAS Annual Meeting*, volume 1, pages 55–60 vol.1, 1995. DOI: 10.1109/IAS.1995.530283.
- [14] Yong Li, Hao Wu, Xing Xu, Xiaodong Sun, and Jindong Zhao. Rotor position estimation approaches for sensorless control of permanent magnet traction motor in electric vehicles: A review. *World Electric Vehicle Journal*, 12:9, 01 2021. DOI: 10.3390/wevj12010009.
- [15] Rongfu Luo, Zenghui Wang, and Yanxia Sun. Optimized luenberger observer-based pmsm sensorless control by pso. *Modelling and Simulation in Engineering*, 2022:3328719, Aug 2022. ISSN 1687-5591. DOI: 10.1155/2022/3328719. URL <https://doi.org/10.1155/2022/3328719>.

- [16] Arafa Mohamed, Mohamed Zaky, Ashraf Din, and Hinza Yasin. Comparative study of sensorless control methods of pmsm drives. 2, 10 2011.
- [17] Mahdi Naderian, Gholamreza Arab Markadeh, Masoud Karimi-Ghartemani, and Mohsen Mojiri. Improved sensorless control strategy for ipmsm using an epll approach with high-frequency injection. *IEEE Transactions on Industrial Electronics*, 71(3):2231–2241, 2024. DOI: 10.1109/TIE.2023.3270528.
- [18] U.-H. Rieder, M. Schroedl, and A. Ebner. Sensorless control of an external rotor pmsm in the whole speed range including standstill using dc-link measurements only. In *2004 IEEE 35th Annual Power Electronics Specialists Conference (IEEE Cat. No.04CH37551)*, volume 2, pages 1280–1285 Vol.2, 2004. DOI: 10.1109/PESC.2004.1355606.
- [19] P.B. Schmidt, M.L. Gasperi, G. Ray, and A.H. Wijenayake. Initial rotor angle detection of a nonsalient pole permanent magnet synchronous machine. In *IAS '97. Conference Record of the 1997 IEEE Industry Applications Conference Thirty-Second IAS Annual Meeting*, volume 1, pages 459–463 vol.1, 1997. DOI: 10.1109/IAS.1997.643063.
- [20] Péter Stumpf. Lecture notes in VIAUM036 Teljesítményelektronika és villamos hajtások: Váltakozó áramú állandómágneses gépek, November 2020.
- [21] Gergely Szabó. *Saliency-based sensorless vector controls of alternating current rotating machines using high-frequency voltage injection methods*. Phd thesis, Budapest University of Technology and Economics, 2022.
- [22] Konrad Urbanski. Estimation of back emf for pmsm at low speed range. *MM Science Journal*, 2015. DOI: 10.17973/MMSJ.2015_03_201506.
- [23] Konrad Urbanski. Determining the observer parameters for back emf estimation for selected types of electrical motors. *Bulletin of the Polish Academy of Sciences, Technical Sciences*, 65, 08 2017. DOI: 10.1515/bpasts-2017-0049.
- [24] Konrad Urbanski and Krzysztof Zawirski. Adaptive observer of rotor speed and position for pmsm sensorless control system. *COMPEL: The International Journal for Computation and Mathematics in Electrical and Electronic Engineering*, 23:1129–1145, 12 2004. DOI: 10.1108/03321640410510848.
- [25] Gaolin Wang, Maria Valla, and Jorge Solsona. Position sensorless permanent magnet synchronous machine drives—a review. *IEEE Transactions on Industrial Electronics*, 67(7):5830–5842, 2020. DOI: 10.1109/TIE.2019.2955409.

- [26] Yi Wang, Ningning Guo, Jianguo Zhu, Nana Duan, Shuhong Wang, Youguang Guo, Wei Xu, and Yongjian Li. Initial rotor position and magnetic polarity identification of pm synchronous machine based on nonlinear machine model and finite element analysis. *IEEE Transactions on Magnetics*, 46(6):2016–2019, 2010. DOI: 10.1109/TMAG.2010.2042690.
- [27] Dan Xiao, Gilbert Foo, and M. F. Rahman. Sensorless direct torque and flux control for matrix converter ipm synchronous motor drives using adaptive sliding mode observer combined with high frequency signal injection. In *2009 IEEE Energy Conversion Congress and Exposition*, pages 4000–4007, 2009. DOI: 10.1109/ECCE.2009.5316521.
- [28] Yin Yan, Jianguo Zhu, and Youguang Guo. A direct torque controlled surface mounted pmsm drive with initial rotor position estimation based on structural and saturation saliencies. In *2007 IEEE Industry Applications Annual Meeting*, pages 683–689, 2007. DOI: 10.1109/07IAS.2007.108.
- [29] Driss Yousfi, Abdelouadoud Halelfadl, and Mohammed El Kard. Sensorless control of permanent magnet synchronous motor. In *2009 International Conference on Multimedia Computing and Systems*, pages 341–344, 2009. DOI: 10.1109/MMCS.2009.5256677.